Geochemistry, Geophysics, Geosystems®

RESEARCH ARTICLE
10.1029/2021GC010101

Special Section:
A fresh look at the Caribbean plate geosystems

Reconstructing the Crustal Section of the Intra-Oceanic Caribbean Island Arc: Constraints From the Cumulate Layered Gabbronorites and Pyroxenites of the Rio Boba Plutonic Sequence, Northern Dominican Republic

J. Escuder-Viruete[1], M. Castillo-Carrión[1], F. Pérez Valera[2], P. Valverde-Vaquero[1], Á. Rubio Ordónez[3], and F. J. Fernández[3]

[1]Instituto Geológico y Minero España – CSIC, Madrid, Spain, [2]Departamento de Ciencias de la Tierra y del Medio Ambiente, Universidad de Alicante, Alicante, Spain, [3]Departamento de Geología, Universidad de Oviedo, Oviedo, Spain

Key Points:

- The Rio Boba mafic-ultramafic plutonic sequence is a lower crust section of the Caribbean island arc
- It is made up by gabbroic rocks and subordinate lenses of pyroxenite
- Their magmatic evolution record subduction initiation and subsequent arc building

Supporting Information:

Supporting Information may be found in the online version of this article.

Correspondence to:

J. Escuder-Viruete,
javier.escuder@csic.es

Citation:

Escuder-Viruete, J., Castillo-Carrión, M., Pérez Valera, F., Valverde-Vaquero, P., Rubio Ordónez, Á., & Fernández, F. J. (2022). Reconstructing the crustal section of the intra-oceanic Caribbean island arc: Constraints from the cumulate layered gabbronorites and pyroxenites of the Rio Boba plutonic sequence, northern Dominican Republic. *Geochemistry, Geophysics, Geosystems*, *23*, e2021GC010101. https://doi.org/10.1029/2021GC010101

Received 16 AUG 2021
Accepted 27 DEC 2021

Author Contributions:

Conceptualization: J. Escuder-Viruete
Formal analysis: J. Escuder-Viruete, M. Castillo-Carrión, F. Pérez Valera, P. Valverde-Vaquero, Á. Rubio Ordónez, F. J. Fernández
Funding acquisition: J. Escuder-Viruete
Investigation: J. Escuder-Viruete, M. Castillo-Carrión, F. Pérez Valera, P.

Abstract Located in northern Dominican Republic, the Early Cretaceous Rio Boba mafic-ultramafic plutonic sequence constitutes a lower crust section of the Caribbean island arc, made up by gabbroic rocks and subordinate pyroxenite. Modal compositions, mineral chemistry, whole-rock compositions and thermobarometric calculations indicate that pyroxenites and gabbronorites represent a cumulate sequence formed by fractionation of tholeiitic magmas with initially very low H_2O content in the lower crust of the arc (0.6–0.8 GPa). Melts evolved along a simplified crystallization sequence of olivine → pyroxenes → plagioclase → Fe-Ti oxides. The magmatic evolution of the Rio Boba sequence and associated supra-crustal Puerca Gorda metavolcanic rocks is multi-stage and involves the generation of magmas from melting of different sources in a supra-subduction zone setting. The first stage included the formation of a highly depleted substrate as result of decompressional melting of a refractory mantle source, represented by a cumulate sequence of LREE-depleted island arc tholeiitic (IAT) and boninitic gabbronorites and pyroxenites. The second stage involved volumetrically subordinate cumulate troctolites and gabbros, which are not penetratively deformed. The mantle source was refractory and enriched by a LILE-rich hydrous fluid derived from a subducting slab and/or overlying sediments, and possibly by a LREE-rich melt. The third stage is recorded in the upper crust of the arc by the Puerca Gorda "normal" IAT protoliths, which are derived from an N-MORB mantle source enriched with a strong subduction component. This magmatic evolution has implications for unraveling the processes responsible for subduction initiation and subsequent building of the Caribbean island arc.

Plain Language Summary The process of intra-oceanic subduction brings an oceanic slab under an overriding oceanic slab resulting in the formation of a convergent plate margin. Consequently, an oceanic island arc is formed in the upper plate, as is the case of the magmatically active arcs of southwest Pacific. Unlike continental magmatic arcs, intra-oceanic arcs are less studied because a large part of them is located below sea level, emerging as chains of small islands that constitute just the tops of large submarine volcanoes. In the northern Dominican Republic, recent geochemical studies of the Caribbean volcanic and plutonic rocks indicate that older tholeiitic and boninitic melts were successively replaced by younger island arc tholeiitic melts. This change in the compositional magmas, as well as related mantle sources, places important constraints on the magmatic and tectonic processes associated with the initiation and evolution of the Caribbean island arc. In this sense, the results presented in this work allow to be compared with the chemical stratigraphy observed in actual oceanic arcs and with the predictions of models for the initiation of intra-oceanic subduction, which constitutes one of the main questions not completely resolved of the global plate tectonics.

1. Introduction

The process of intra-oceanic subduction brings an oceanic slab under an overriding oceanic slab resulting in the formation of a convergent plate margin. Consequently, an oceanic island arc is formed in the upper plate, as is the case of the magmatically active arcs of Izu-Bonin-Mariana, South Sandwich and Lesser Antilles (Arculus et al., 2015; Leat & Larter, 2003; Stern, 2010). Unlike continental magmatic arcs, intra-oceanic arcs are less studied because a large part of them is located below sea level, emerging as chains of small islands that constitute just the tops of large submarine volcanoes. Despite these difficulties, the magmatic processes in intra-oceanic arcs have been directly and indirectly studied from: (a) lower crust and upper mantle xenoliths erupted in

Valverde-Vaquero, Á. Rubio Ordónez, F. J. Fernández
Methodology: J. Escuder-Viruete, M. Castillo-Carrión
Project Administration: J. Escuder-Viruete
Writing – original draft: J. Escuder-Viruete
Writing – review & editing: J. Escuder-Viruete, M. Castillo-Carrión, P. Valverde-Vaquero, F. J. Fernández

active volcanoes (DeBari & Greene, 2011; McInnes et al., 2001); (b) diving, dredging and drilling partial crustal exposures on the deep sea floor (Ishizuka et al., 2006; Pearce et al., 1992; Reagan et al., 2010, 2019; Taylor et al., 1994); and (c) from geophysical surveys of the island arc crust (Calvert, 2011; Takahashi et al., 2008).

Direct evidence of the processes controlling the evolution and formation of volcanic arcs also comes from the obducted sections of intra-oceanic arc lithosphere that form ophiolitic sequences in orogenic belts (Pearce, 2003; Stern et al., 2012). However, examples of well-preserved exhumed arc sections, complete from their mantle roots to upper volcano-sedimentary levels are very scarce. The best studied arc sections probably are: the Jurassic Talkeetna arc in south-central Alaska (DeBari & Greene, 2011; Greene et al., 2006; Kelemen et al., 2014); and the Cretaceous Kohistan arc in northern Pakistan (Bouilhol et al., 2015; Burg, 2011; Dhuime et al., 2007; Garrido et al., 2006, 2007; Jagoutz et al., 2007, 2011, 2018). Both Talkeetna and Kohistan paleo-arcs are compositionally stratified and contain a lower section made up of a basal ultramafic sequence of peridotite and pyroxenite, overlain by a mafic sequence of gabbroic rocks. To explain the genetic link between the ultramafic and mafic sequences two main hypotheses have been proposed.

The first hypothesis suggests that the ultramafic-mafic sequence, composed of dunites, wehrlites, pyroxenites, hornblendites, and gabbronorites, may have crystallized in the upper mantle and lower crust from a single type of primitive arc magma [Mg# >60; where Mg# = molar 100 × Mg/(Mg + Fe_{total})] (DeBari & Greene, 2011; Greene et al., 2006; Kelemen et al., 2014). The existence of primitive gabbronorites and the complementary compositions of the more evolved plutonic and volcanic rocks, together with the rather homogenous Nd-isotopic compositions of diverse igneous units of the arc, are put forward to argue for a common origin (magmatic or cumulative) for the ultramafic and mafic rocks in the crustal section through (simple) fractional crystallization (DeBari & Greene, 2011; Greene et al., 2006; Kelemen et al., 2014; Rioux et al., 2007). Therefore, the gabbronorites would represent the crystallized cumulate pile and the erupted volcanic rocks the residual liquid following differentiation. This hypothesis is supported by experimental studies (e.g., Müntener & Ulmer, 2018; Müntener et al., 2001; Villiger et al., 2007, 2004), which successfully reproduced the formation of high-Mg# pyroxenites and complementary low-Mg# melts during the crystallization of anhydrous primitive magmas at lowermost arc crust conditions.

In the Kohistan paleo-arc, however, the scarcity of rocks with intermediate Mg# values between high-Mg# dunites-wehrlites-pyroxenites and overlying gabbros, as well as the existence of significant variations in the Sr-Nd-Pb isotope data between these groups of rocks, rule out a simple fractional crystallization relationship between the ultramafic and mafic sequences. These petrological characteristics and REE numerical modeling suggest a second hypothesis for the origin of the ultramafic sequence by melt-rock reaction at the expense of the sub-arc oceanic mantle (Burg, 2011; Dhuime et al., 2007; Garrido et al., 2006, 2007). Although predicted by crystal fractionation models, a thick ultramafic layer of cumulates is nevertheless absent in the crustal section of both arcs. This absence has been interpreted as a consequence of delamination of dense, unstable lower crust and/or convective thermomechanical erosion of the sub-arc lithosphere (Dhuime et al., 2007; Garrido et al., 2006, 2007; Jull & Kelemen, 2001; Kelemen et al., 2014). Later studies establish a more complex magmatic evolution for the Kohistan arc that includes different mantle sources for the ultramafic and mafic rocks throughout an extended period of ca. 30 Ma. This evolution includes a first stage of extensive boninitic magmatism connected with initiation of subduction, followed by a tholeiitic magmatism second stage associated with the building of a mature arc. This last stage culminates with granitic magmatism that produces intra-crustal differentiation (by fractionation process), associated with delamination and/or erosion of the lower arc crust (DeBari & Greene, 2011; Dhuime et al., 2007; Jagoutz & Schmidt, 2012; Jagoutz et al., 2011, 2018; Stern, 2010).

A multi-stage tectono-magmatic evolution has also been proposed to explain the characteristics of the mantle and crustal sections of the Puerto Plata ophiolitic complex (PPC), which constitutes a segment of the Caribbean, intra-oceanic island arc in northern Dominican Republic (Figure 1; Escuder-Viruete et al., 2006, 2014). Currently preserved at several places in the Greater Antilles, the Caribbean island arc contains volcanic rocks as old as Late Aptian to Lower Albian (Escuder-Viruete et al., 2006, 2014; Hastie et al., 2013; Jolly et al., 2006; Kesler et al., 2005; Lewis et al., 2002; Marchesi et al., 2006; Proenza et al., 2006; Rojas-Agramonte et al., 2011, 2016; Torró et al., 2017). Following Draper et al. (1994), the arc is generally interpreted to have formed in a supra subduction zone (SSZ) setting at the leading edge of the Caribbean plate by SW-directed subduction (present-day coordinates) of the proto-Caribbean lithosphere.

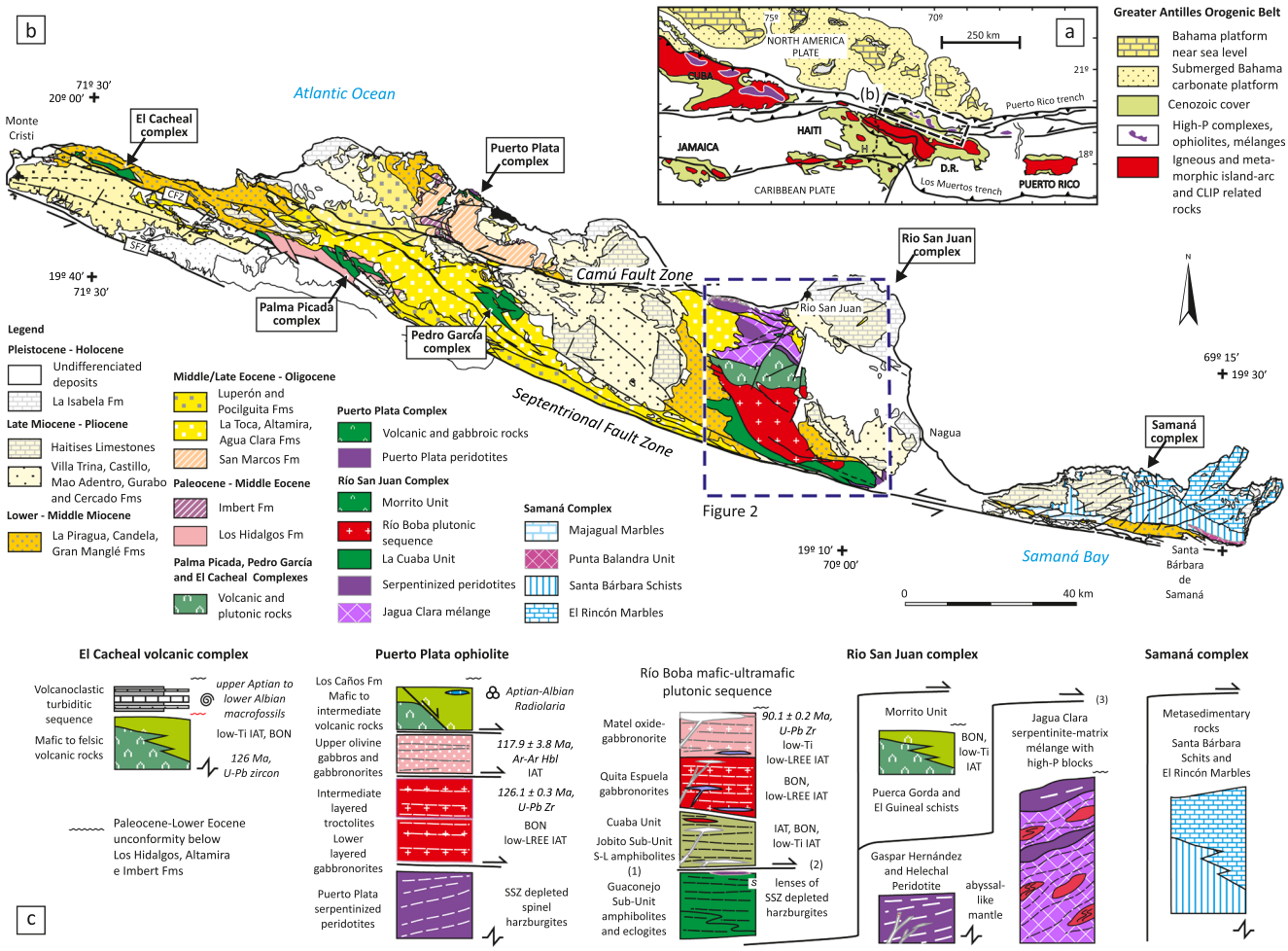

Figure 1. (a) Map of the northeastern Caribbean plate margin. Box shows location of the northern Hispaniola area. DR, Dominican Republic. (b) Geological map of Septentrional Cordillera and Samaná Peninsula modified from Draper and Nagle (1991), Draper et al. (1994), Escuder-Viruete, Pérez-Estaún, Gabites, et al. (2011), and Escuder-Viruete, Valverde-Vaquero, Rojas-Agramonte, Gabites, & Pérez-Estaún, 2013. SFZ, Septentrional fault zone. (c) Schematic lithologic sections of the Cretaceous igneous and metamorphic complexes of the Caribbean subduction-accretionary prism discussed in the text (Escuder-Viruete, Valverde-Vaquero, Rojas-Agramonte, Gabites, & Pérez-Estaún, 2013; Escuder-Viruete, Valverde-Vaquero, Rojas-Agramonte, Jabites, et al., 2013). IAT, island-arc tholeiite; BON, boninitic rocks; (1) large-scale extensional shear zone (91–85 Ma); (2) Jobito late detachment (75–71 Ma); and (3) syn-collisional thrusts (Maastrichtian-Lower Eocene).

In the northern Dominican Republic, geochemical studies of the Caribbean volcanic rocks indicate that older LREE-depleted tholeiitic and boninitic melts were successively replaced by younger island arc tholeiitic (IAT) melts (Escuder-Viruete et al., 2006, 2014). This change in the compositional magmas, as well as related mantle sources, places important constraints on the magmatic and tectonic processes associated with the initiation and evolution of the Caribbean island arc. These changes coincide with the chemical stratigraphy observed in actual oceanic arcs (Ishikawa et al., 2002, 2006, 2011; Reagan et al., 2010, 2019) and with models for the initiation of intra-oceanic subduction (see review in Stern & Gerya, 2018). Recent advances in regional geological knowledge have made it possible to identify the plutonic rocks that constitute the lower crust of the Caribbean arc and their complementary volcanic rocks in the upper crust, which have been very little studied (Escuder-Viruete & Castillo-Carrión, 2016; Escuder-Viruete, Valverde-Vaquero, Rojas-Agramonte, Gabites, & Pérez-Estaún, 2013).

Here, we combine field mapping, petrological, mineralogical and geochemical data in order to characterize the lower crust of the Caribbean island arc exposed in the Rio Boba mafic-ultramafic plutonic sequence in the northern Dominican Republic. The main objective is to establish the petrogenetic relationships among the cumulate pyroxenites and gabbronorites of the plutonic complex, and the structurally adjacent mafic metavolcanic rocks of the Puerca Gorda Schists, which are representative of the volcanic rocks of the upper arc crust. These relationships allow us to (a) constraint the main differentiation processes in the magmatic system, (b) reconstruct the

crustal section of the intra-oceanic Caribbean island arc, (c) place constraints on the nature of parental magmas during subduction zone infancy, and (d) propose regional correlations based on a spatial/temporal evolution in stages for the arc magmatism. The obtained results allow us to propose a multi-stage tectono-magmatic model, in which the birth and subsequent evolution of the Caribbean island arc was controlled by the generation of magmas from melting of different sources in an extensional supra-subduction zone setting.

2. Geological Setting

2.1. From Intra-Oceanic Subduction to Arc-Continent Collision in the Northern Caribbean Plate

Located on the northern margin of the Caribbean plate, the geology of Hispaniola (Dominican Republic and Haiti; Figure 1) is the result of the SW-directed Cretaceous subduction to final oblique collision in the lower Eocene of the Caribbean intra-oceanic arc with the southern continental margin of North American (Draper et al., 1994; Escuder-Viruete, Pérez-Estaún, Booth-Rea, et al., 2011; Escuder-Viruete, Valverde-Vaquero, Rojas-Agramonte, Gabites, & Pérez-Estaún, 2013; Escuder-Viruete, Pérez-Estaún, Gabites, et al., 2011; Escuder-Viruete, Valverde-Vaquero, Rojas-Agramonte, Jabites, et al., 2013; Mann et al., 1991; Pérez-Estaún et al., 2007). Occurrence of high-P mélanges and ophiolites in northern Hispaniola indicates that an intermediate proto-Caribbean oceanic basin was subducted at least since the Lower Cretaceous (Draper & Nagle, 1991; Escuder-Viruete, Friedman, et al., 2011; Escuder-Viruete & Pérez-Estaún, 2013; Krebs et al., 2011). Volcanic and shallow plutonic rocks whose ages range from the Aptian to the lower Eocene record the magmatic activity in the Caribbean upper plate (Escuder-Viruete et al., 2006, 2014; Kesler et al., 2005; Torró et al., 2017, 2018). A cover of middle to upper Eocene to Holocene sedimentary rocks regionally overlies the arc-related rocks. This cover post-dates the magmatic island arc activity and records the oblique arc-continent collision in northern Hispaniola, as well as intra- and back-arc deformation in the central and southern areas of the island (Pérez-Estaún et al., 2007).

In northern Hispaniola (Figure 1), the pre-collisional geologic history is recorded in the pre-Eocene igneous and metamorphic basement, which crops out in several inliers, termed El Cacheal, Palma Picada, Pedro García, Puerto Plata, Río San Juan, and Samaná complexes (Draper & Nagle, 1991). These complexes make up a segment of the Caribbean subduction-accretionary prism (Escuder-Viruete, Pérez-Estaún, Gabites, et al., 2011; Escuder-Viruete, Valverde-Vaquero, Rojas-Agramonte, Gabites, & Pérez-Estaún, 2013; Escuder-Viruete, Valverde-Vaquero, Rojas-Agramonte, Jabites, et al., 2013), including from lower to upper structural levels: metasediments of the subducted continental margin of North America (Samaná complex); ophiolitic fragments of the proto-Caribbean Ocean (northern Río San Juan complex); serpentinitic-matrix mélanges enclosing high-P blocks of the subduction channel (Jagua Clara mélange); and volcano-plutonic rocks of the Caribbean island arc and fore-arc (southern Río San Juan, Pedro García, Palma Picada, Puerto Plata, and El Cacheal complexes). The eastward and structurally downward younging age of the main deformation in each structural unit reflects their progressive accretion to the Caribbean subduction-accretionary prism from the latest Cretaceous to the lower Miocene (Escuder-Viruete, Pérez-Estaún, Booth-Rea, et al., 2011; Escuder-Viruete, Valverde-Vaquero, Rojas-Agramonte, Jabites, et al., 2013). During the middle Miocene, the tectonic regime changes from oblique arc-continent collision to crustal-scale strike-slip faulting and eastward escape of the Caribbean plate toward a collision-free side in the Atlantic Ocean (Draper et al., 1994; Escuder-Viruete & Pérez, 2020; Mann et al., 1991). Still active in northern Hispaniola, this tectonic regime gave rise to transpressive tectonics, tectonic disruption, and lateral escape of blocks of the Caribbean subduction-accretionary prism (Escuder Viruete et al., 2020).

2.2. Main Structural Subdivision of the Rio San Juan Complex

The Rio San Juan complex consists of Mesozoic igneous and metamorphic rocks, which are peripherally surrounded by a folded and faulted unconformable cover of Paleocene to middle Miocene sedimentary rocks, and locally capped by a subhorizontal Miocene to Pleistocene reef limestone (Figure 2). The large-scale internal ductile deformation of the complex consists of a SW-dipping nappe pile (Escuder-Viruete, Valverde-Vaquero, Rojas-Agramonte, Gabites, & Pérez-Estaún, 2013). In ascending structural order, it includes (see Supporting Information S1 for more detail): the Gaspar Hernández and Helechal peridotites, the Jagua Clara serpentinite-matrix mélange, the Morrito and Cuaba units, and the Rio Boba mafic-ultramafic plutonic sequence, which is the object of this contribution. The last three units belong to the Caribbean upper plate of the subduction-accretionary prism.

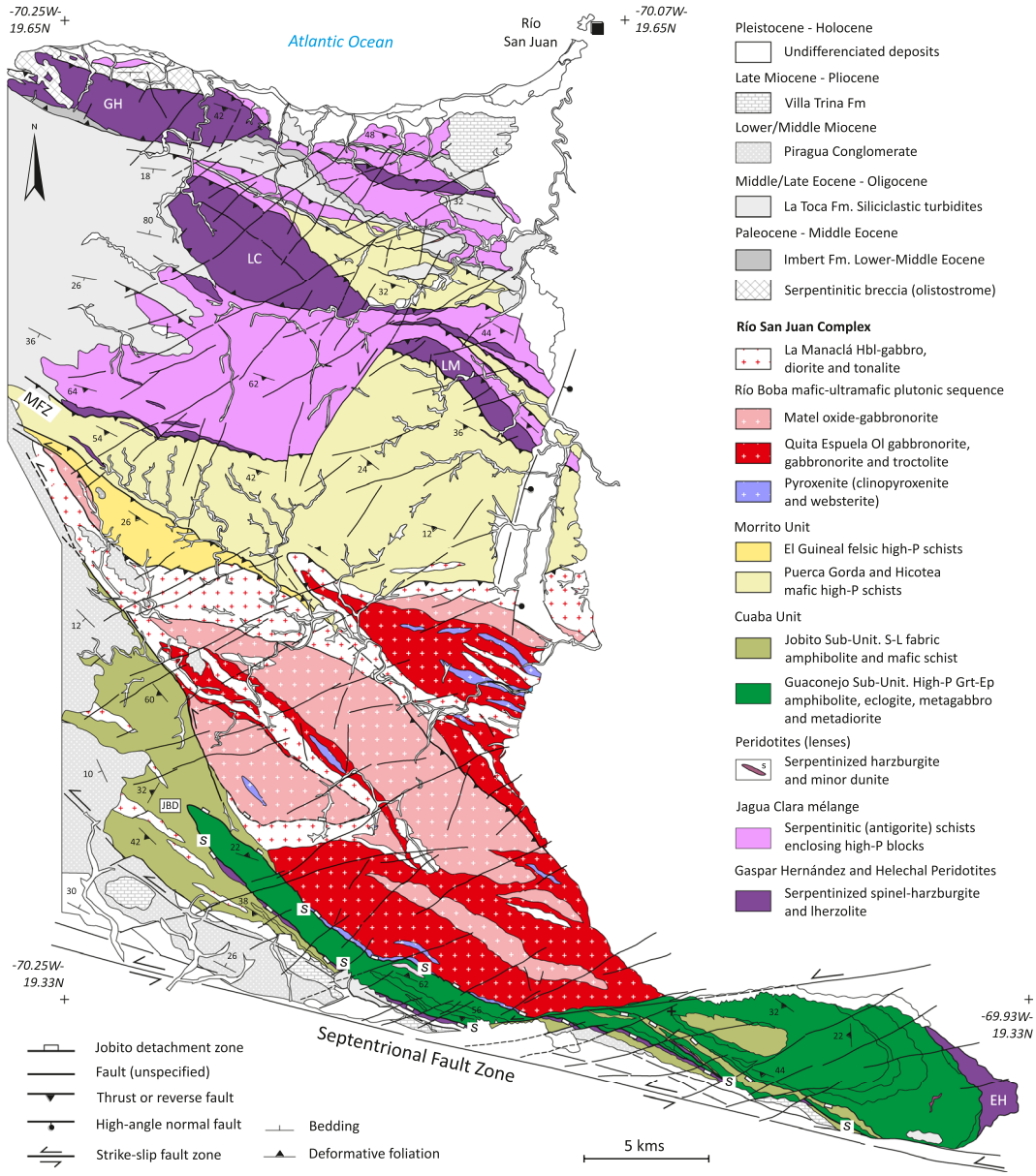

Figure 2. Simplified geological map of Río San Juan complex modified from Draper and Nagle (1991), Escuder-Viruete, Valverde-Vaquero, Rojas-Agramonte, Gabites, and Pérez-Estaún (2013), Escuder-Viruete, Valverde-Vaquero, Rojas-Agramonte, Jabites, et al. (2013), showing major lithological units, neogene brittle structures, and representative structural attitudes of rocks. The late Jobito basal detachment juxtaposes the upper Jobito and lower Guaconejo structural subunits. The Morrito fault zone emplaced the blueschist nappe on top of the Jagua Clara high-P mélange. Locations of serpentinized peridotite lenses (s) are indicated. Peridotite massifs: GH, Gaspar Hernández; LC, Loma Catey; LM, Loma El Morrito; and EH, Helechal.

In the northern Río San Juan complex, the Gaspar Hernández peridotite forms km-scale tectonic blocks of harzburgite and lherzolite, variably replaced by a low-T chrysotile-lizardite assemblages, intruded by gabbro sills of N-MORB chemistry and Lower Cretaceous age. In the SE sector of the complex, the Helechal peridotite forms a tectonic slice of peridotites of a similar, abyssal-like composition, which have structural continuity along a km-scale synform under the Cuaba and Morrito units. Both peridotite units have been interpreted as fragments of the proto-Caribbean oceanic lithosphere, consumed by subduction below the Caribbean island arc (Escuder-Viruete, Friedman, et al., 2011).

The Jagua Clara mélange consists of foliated antigorite mainly, which warps around blocks of high-P rocks (Escuder-Viruete & Pérez-Estaún, 2013; Krebs et al., 2011). The mélange contains mafic blocks plucked from both the upper plate (arc-like protoliths, Caribbean island arc) and the lower plate (N-MORB protoliths, proto-Caribbean Ocean), suggesting that the Jagua Clara serpentinite-matrix mélange represents the deep subduction channel, formed during intra-oceanic subduction.

In the southern Río San Juan complex, the Morrito unit is composed of the Puerca Gorda Schists in the lower structural levels and the El Guineal Schists in the upper ones (Draper & Nagle, 1991). The mafic protoliths of Puerca Gorda Schists were heterogeneously deformed and metamorphosed to blueschist- and greenschist-facies conditions during arc-continent convergence. However, toward the upper structural levels, the strain intensity decreases and the unit consists of porphyritic, aphyric and vesicular (amygdaloidal) mafic-intermediate volcanic flows. On a microscopic scale, these volcanics rocks preserve pyroxene-phyric/microphyric and variolitic quench volcanic textures. Euhedral/subhedral orthopyroxene and clinopyroxene are the most abundant phenocrysts followed by subhedral plagioclase. Mafic volcanic protoliths derived from boninite, low-Ti IAT, and IAT type magmas (Escuder-Viruete, Friedman, et al., 2011). The Guineal Schists derived from dacitic to rhyolite protoliths and have provided SHRIMP zircon core ages of 122.2 and 121.7 Ma (Escuder-Viruete, 2010). In less deformed domains, quartz and feldspar-phyric volcanic textures are preserved. Based on major and trace element compositional data, Escuder-Viruete, Friedman, et al. (2011) concluded that the metavolcanic rocks of the Morrito unit represent the volcanic part of the Caribbean fore-arc. The Morrito basal thrust juxtaposes the Puerca Gorda Schists northward onto the Jagua Clara serpentinite-matrix mélange. This juxtaposition took place in the latest Maastrichtian to Paleocene, at the onset of the arc-continent collision (Escuder-Viruete, Valverde-Vaquero, Rojas-Agramonte, Gabites, & Pérez-Estaún, 2013; Escuder-Viruete, Valverde-Vaquero, Rojas-Agramonte, Jabites, et al., 2013).

The Cuaba unit is composed of two coherent tectonometamorphic assemblages (Figure 2). The structurally uppermost Jobito assemblage consists of foliated and mylonitized metabasites metamorphosed to low-P amphibolite-facies conditions. The underlaying Guaconejo assemblage is made up of garnet-epidote amphibolites, mafic eclogites and heterogeneous coarse-grained garnet-bearing and garnet-free orthogneisses (metaultramafic cumulates, metagabbros, and metadiorites) metamorphosed to upper amphibolite and eclogite-facies conditions (Abbott et al., 2007; Escuder-Viruete & Pérez-Estaún, 2013). Blocks of garnet-bearing ultramafic rocks are a distinct component of the Guaconejo assemblage. Their magmatic mineral assemblages record a liquid line of descent (by fractional crystallization) consistent with mantle conditions (>3.2 GPa; Abbott & Draper, 2013; Gazel et al., 2011). A low-pressure alternative origin for the garnet-bearing ultramafic rocks has also been proposed (Hattori, Guillot, Saumur, et al., 2010; Hattori, Guillot, Tubrett, et al., 2010). Mafic protoliths of the Cuaba unit originated from boninite, low-Ti IAT, and IAT type magmas (Escuder-Viruete & Castillo-Carrión, 2016; Escuder-Viruete, Friedman, et al., 2011), suggesting that this unit represents part of the subducted fore-arc of the Caribbean island arc. Abbott and Draper (2013) describe eclogites derived from related N-MORB protoliths in the Cuaba unit, probably derived from subducted oceanic lithosphere and later exhumed in the subduction channel. The Jobito and Guaconejo assemblages are tectonically juxtaposed by a Campanian to Maastrichtian (~75–70 Ma) late retrograde detachment zone, which is marked by several rootless bodies of serpentinized peridotites, compositionally similar to SSZ mantle (Figure 2). A basal section of mafic-ultramafic cumulates is lacking. The Guaconejo assemblage is also tectonically juxtaposed against the underlaying Helechal peridotites.

The uppermost Rio Boba mafic-ultramafic plutonic sequence includes three main cartographic units (Figure 2): Quita Espuela layered gabbronorites; Matel oxide gabbronorites; and La Manaclá hornblende gabbros, diorites and tonalities. Outcrop conditions under a tropical climate are generally very poor. Gabbroic rocks are in occasions deformed and recrystallized to a two-pyroxene granulite, but the meta-prefix is omitted hereafter for simplicity. The metamorphic evolution of the plutonic complex will be presented in a separate publication. The Cuaba unit, the Puerca Gorda Schists and the Rio Boba plutonic sequence were intruded by syn-kinematic hornblende-bearing tonalites during the Late Cretaceous (90.1 ± 0.2 Ma; U-Pb in zircon; Escuder-Viruete, Valverde-Vaquero, Rojas-Agramonte, Jabites, et al., 2013).

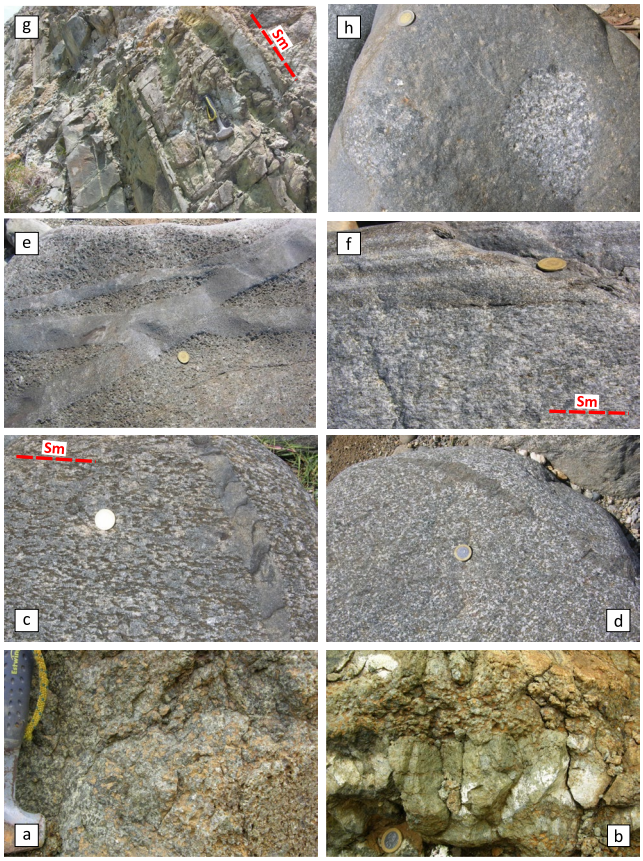

Figure 3. Field features of pyroxenites and gabbronorites from the Rio Boba plutonic sequence. (a) Cumulate texture in olivine websterite. Width of view = 35 cm. (b) Alternating layers at centimeter scale of clinopyroxenite and olivine clinopyroxenite. The coin is 2.5 cm in diameter. (c) High-temperature foliation (Sm) in deformed gabbronorites defined by the preferential mineral orientation, ductile stretching and microboudinage of the pyroxene and plagioclase aggregate. Note the high-angle intrusion of an undeformed gabbronorite dike. (d) Cumulate texture in coarse-grained gabbronorite, which is intruded by a pyroxenite vein. (e) Layered gabbronorite intruded by anatamosing dikes of undeformed oxide gabbronorite. (f) Modal layering in gabbronorites (Sm), defined by variations of the mafic mineral/plagioclase ratio at the millimeter to decimeter scale. (g) Matel oxide gabbronorite characterized by development of a penetrative magmatic to solid-state deformative foliation (Sm). Width of view = 2.5 m. (h) Massive troctolite with cumulate igneous texture containing centimeter-size enclaves of foliated gabbronorite.

3. The Rio Boba Mafic-Ultramafic Plutonic Sequence: Field Relations and Petrography

The Rio Boba mafic-ultramafic plutonic sequence is a lenticular massif, whose approximate dimensions are 30 km long and 15 km wide, composed of gabbroic rocks and subordinate lenses of pyroxenite (Figure 2 and Supporting Information S1). Cross-sections show that the southern Rio San Juan complex is folded by late WNW-ESE trending, subvertical antiforms and synforms of kilometer wavelength, which fold on a regional scale the main foliation in the different units and the magmatic and solid-state deformation fabrics in the Rio Boba plutonic sequence (Escuder-Viruete, Valverde-Vaquero, Rojas-Agramonte, Gabites, & Pérez-Estaún, 2013). The plutonic sequence is overprinted by late thrust, reverse, and strike-slip faults related to Neogene transpressive tectonics.

3.1. Pyroxenites

The pyroxenite lenticular bodies can be recognized in the field by their fresh appearance, green to orange color, and medium-to-coarse grained cumulate texture (Figure 3a). In map view (Figure 2), these lenses are 0.5–2.5 km long and 0.1–0.3 km wide. Their composition varies from pure clinopyroxenite to websterite with an approximate orthopyroxene/clinopyroxene ratio of 1:3. The olivine varieties (up to 25 vol.%) are made of olivine clinopyroxenite and olivine websterite (Figure 4b). In some samples, plagioclase (<3 vol.%, hereinafter %) is interstitial. Pyroxenite bodies are internally composed of alternating meter scale to millimeter scale layers of clinopyroxenite with clinopyroxene-dominant websterite and olivine clinopyroxenite with subordinate olivine websterite (Figure 3b). Contacts between pyroxenites and nearby gabbroic rocks are not exposed. The pyroxenites commonly do not show a deformational fabric, but recrystallization is indicated in some samples by porphyroblasts in thin section.

Clinopyroxenite and olivine clinopyroxenite are medium- to coarse-grained and display a hypidiomorphic to idiomorphic granular to granoblastic texture. They contain unaltered green clinopyroxene (92%–99%) with olivine (0%–8%), minor orthopyroxene (0%–8%), and green spinel (<2%). Clinopyroxene textures range from euhedral adcumulate to mesocumulate (Figure 5b) and granoblastic, where smaller recrystallized polygonal grains surround large magmatic clinopyroxene grains. Exsolution of orthopyroxene in clinopyroxene is ubiquitous. Orthopyroxene is subhedral. Olivine forms large subhedral grains or occurs as an equigranular polygonal mosaic (Figure 5a). Spinel occurs as discrete grains and as exsolution lamellae in clinopyroxene.

Websterite and olivine websterite are medium-to coarse-grained and range from adcumulate to orthocumulate and recrystallized granoblastic in texture. They are composed of 65%–75% clinopyroxene that has exsolution lamellae of orthopyroxene, and 25%–35% orthopyroxene with a pink-green pleochroism and exsolution lamellae of clinopyroxene (Figure 4b). Olivine forms large subhedral grains (0%–22%). Relic igneous textures indicate adcumulus growth. In recrystallized rocks, orthopyroxene and clinopyroxene form intergrowths with curved cuspate contacts. Euhedral Mg-Al spinel is rare (<1%) and has a slight greenish tint. Plagioclase occurs as an intercumulus phase forming a subequigranular mosaic (<5%). Plagioclase-bearing websterite also appears as centimeter scale pockets in the massive websterite.

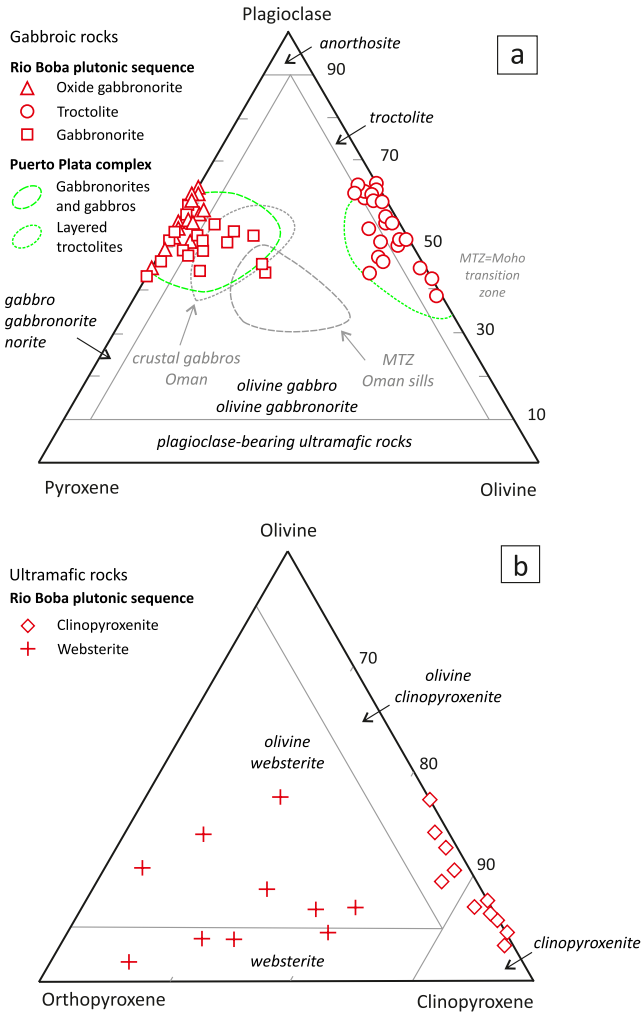

Figure 4. Rio Boba plutonic sequence. (a) Modal compositions of the gabbroic rocks compared to those of the lower and middle crustal gabbros and Moho Transition Zone sills of the Oman ophiolite and the Puerto Plata ophiolite complex (compiled by Escuder-Viruete et al., 2014; Marchesi et al., 2006). (b) Modal compositions of the ultramafic. See text for explanation.

3.2. Gabbroic Rocks

The gabbroic rocks of the Rio Boba sequence form a stack of kilometer-thick sills, in which the underlaying Quita Espuela gabbronorites are compositionally different than the overlaying oxide-rich Matel gabbronorites (Figure 2). The Quita Espuela gabbronorite is a 0.8–1.6 km-thick unit, mainly composed of medium-to coarse-grained layered spinel-bearing gabbronorite and olivine gabbronorite, with subordinate troctolite and olivine gabbro (Figure 4a). In the field, the contact between the different gabbroic rocks is gradacional. The compositional layering is defined by variations of the mafic mineral/plagioclase ratio at the millimeter to meter scale (Figure 3f), or by grain-size graded layers. The layering is generally oriented WNW-ESE to NW-SE and dip a low angle (<30°) to the NE and SW. It is often sheared, boudinaged, and locally isoclinally folded, suggesting deformation and foliation development at high-temperature (Figure 3c).

The least deformed Quita Espuela gabbronorites exhibit in thin section an orthocumulate to partly equilibrated granoblastic texture with interpenetrated grain boundaries (2–10 mm; Figure 5d). They have an anhydrous association of clinopyroxene (15%–35%), brownish orthopyroxene (5%–25%), plagioclase (30%–65%), olivine (0%–15%), and green spinel (<8%). Relict igneous cumulate textures indicate ortho-to adcumulus growth. Clinopyroxene contains exsolution lamellae of orthopyroxene, and vice versa. Zoning has not been detected in any of the phases. Green spinel (hercynite) or Fe-Ti oxides (magnetite-ilmenite) occurs interstitially. Some undeformed gabbronorites are characterized by coronitic shells of orthopyroxene and Fe-Ti oxide around olivine at the contact with plagioclase. Deformed gabbronorite exhibits a penetrative grain-shape defined by polycrystalline ellipsoidal clusters of pyroxene alternating with bands of elongate plagioclase grains (Figure 5c). The grain boundaries range from straight to lobate. Lobate grain boundaries are indicative of dynamic recrystallization at relatively high-temperatures (Passchier & Trouw, 2005). In these deformed rocks, green-brown calcic amphibole (0%–15%) poikilitically enclose both orthopyroxene and clinopyroxene.

Overlaying and interleaved with the layered gabbronorites there is a 75–200 m-thick unit of coarse-grained, layered troctolite, subordinate olivine gabbro, and rare gabbroic anorthosite (volume <10%, approximately). These rocks preserve cumulate igneous textures and contain rare centimeter-scale enclaves of foliated gabbronorite (Figure 3h). Undeformed troctolite has orthocumulate texture, and commonly exhibits layer-parallel, preferred orientations defined by plagioclase laths and elongated olivine. Troctolite has variable proportions of plagioclase (45%–90%), but rocks with around 65% plagioclase and 35% olivine are particularly abundant. Plagioclase is subhedral, 0.2–1.5 cm sized and locally recrystallized into polygonal aggregates. It contains inclusions of idiomorphic olivine (Figure 5f). Olivine is 0.5–5 mm long, sub-to euhedral, variably serpentinized and locally surrounded by coronitic shells of orthopyroxene and Fe-Ti oxide. Some undeformed troctolites are characterized by clinopyroxene-spinel and amphibole-spinel symplectites at the olivine-plagioclase interface (Figure 5e). Associated olivine gabbros are cumulates dominated by plagioclase and clinopyroxene, with minor olivine. In these rocks, olivine (<25%) forms 0.5–1.5 mm grains dispersed between dominant subhedral plagioclase (45%–70%) and clinopyroxene (20%–35%). Orthopyroxene (<15%) is generally interstitial between plagioclase laths and clinopyroxene. Magnetite is the only oxide present.

The Matel gabbronorites is 0.6–1.2 km-thick unit composed of medium-to fine-grained oxide gabbronorite, oxide gabbro and subordinated diorite. With respect to the underlying Quita Espuela gabbronorites, these rocks are characterized by a higher modal abundance of Fe-Ti oxides and a smaller grain size. Also, they are often characterized by the development of a penetrative magmatic to solid-state foliation, which is flat-lying or dip a

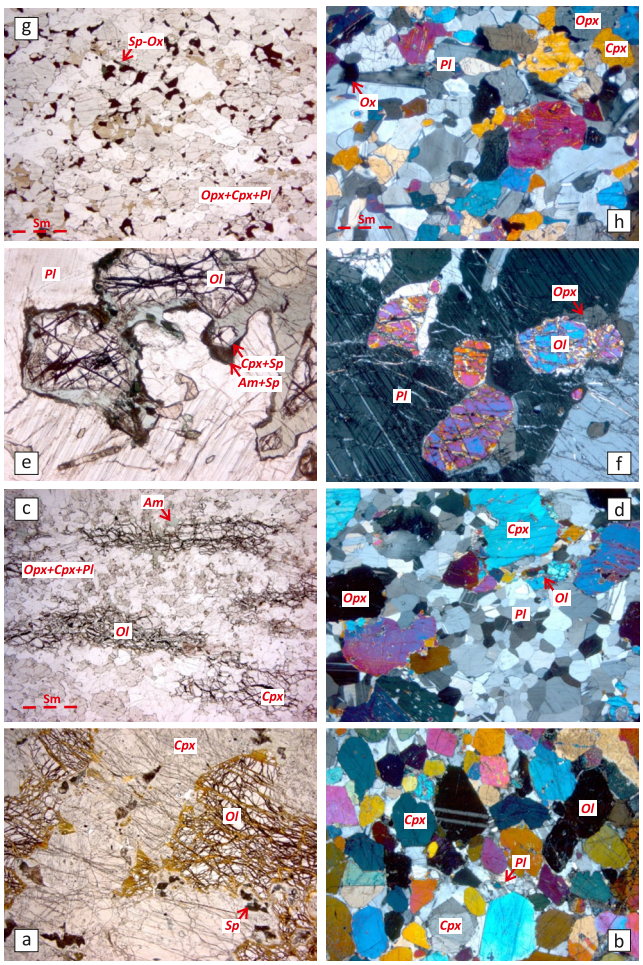

Figure 5. Photomicrographs showing features of the mafic and ultramafic rocks of the Rio Boba sequence. (a) Euhedral olivine (Ol) associated with cumulus clinopyroxene (Cpx) and intercumulus hercynite (Spl) in olivine clinopyroxenite. PPL. (b) Meso to adcumulate texture composed of cumulate clinopyroxene (Cpx) and olivine (Ol) and interstitial plagioclase (Pl) in plagioclase-bearing olivine clinopyroxenite. CPL. (c) High-T deformation fabric (Sm) defined by a recrystallized and elongated aggregates of olivine (Ol), clinopyroxene (Cpx), minor orthopyroxene (Opx), and plagioclase (Pl). Note the minor presence of retrograde calcic amphibole (Am). Quita Espuela lower layered gabbronorites. PPL. (d) Slight deformed and dynamically recrystallized gabbronorite, consisting of varying modal proportions of olivine (Ol), orthopyroxene (Opx), clinopyroxene (Cpx), and plagioclase (Pl). Quita Espuela lower layered gabbronorites, CPL. (e) Zoned clinopyroxene-spinel (Cpx-Spl) and amphibole-spinel (Am-Spl) symplectites at the olivine-plagioclase (Ol-Pl) interface in undeformed troctolites. PPL. (f) Euhedral olivine (Ol) in large cumulus plagioclase (Pl). Olivine is partially rimed by coronitic shells of orthopyroxene (Opx). Quita Espuela troctolites. CPL. (g) Extensive recrystallization of clinopyroxene (Cpx), orthopyroxene (Opx), plagioclase (Pl), and Fe-Ti oxides (Ox) in Matel upper oxide gabbronorites. Preferred mineral elongation defines a sub-solidus foliation (Sm). PPL. (h) Elongated grains with lobate grain boundaries of orthopyroxene (Opx), clinopyroxene (Cpx), plagioclase (Pl), and interstitial Fe-Ti oxide (Ox) defining a sub-solidus foliation (Sm) in Matel upper oxide gabbronorites. CPL. Width of field is 1 cm (c and g) and 5 mm (rest of photomicrographs). Supporting Information S1 contains the same photomicrographs in complementary parallel/cross-polarized light.

low-angle to the NE or SW (Figure 3g). This foliation is sub-concordant to the layering in the underlying Quita Espuela gabbronorites. Less deformed oxide gabbronorites contain rare centimeter-scale enclaves of gabbronorite.

Granoblastic textures in thin section indicate that ductile flow and recrystallization occurred at high-T (Figures 5g and 5h). Recrystallization of clinopyroxene, orthopyroxene and plagioclase results in elongate to equant polygonal textures. Black oxides (5%–15%) occur as tabular shaped grains and are made of magnetite-ilmenite pairs. In the more deformed oxide gabbronorites, a strong foliation is defined by alternating plagioclase-rich and plagioclase-poor bands on a millimeter scale, reinforced by the preferred orientation of Fe-Ti oxide grains. In some samples, spinel is green, anhedral, and occurs interstitially. Amphibole (0%–10%) rims and poikilitically encloses ortho and clinopyroxene. Oxide gabbronorites are characterized by clinopyroxene-spinel, amphibole-spinel, and amphibole-Fe-Ti oxides symplectites around elongated plagioclase and orthopyroxene, suggesting that cooling took place after high-T deformation. The Fe-Ti oxide gabbros are characterized by an elongated granular texture, composed by subhedral 2–5 mm-scale tabular plagioclase and 0.5–8 mm-scale anhedral clinopyroxene.

3.3. Retrograde Metamorphic Mineral Assemblages

Metamorphic overprint is variably developed and depends on the intensity of the retrograde deformation. In less deformed rocks, it is defined by formation of coronitic shells of orthopyroxene ± Fe-oxide around olivine and clinopyroxene + spinel and calcic amphibole + spinel symplectites between olivine and plagioclase. These replacement microstructures record subsolidus cooling in granulite and amphibolite-facies metamorphic conditions. However, retrograde metamorphism and hydrous assemblages becomes more pervasive structurally downward the Rio Boba plutonic sequence, that is, toward the Jobito basal detachment (JBD) zone. In these 250 m-thick lower structural levels, retrograde metamorphism is related to development of a network of amphibolite to upper greenschist-facies mylonitic shear zones and veins, where pyroxene is extensively replaced by green-brown and green calcic amphibole and plagioclase by epidote/clinozoisite, albite and chlorite. In the shear zones, the gabbronorites have been completely recrystallized and transformed into amphibolites, characterized by a well-developed penetrative plane-linear fabric. This metamorphic fabric is sub-parallel to the foliation in the Jobito amphibolites (91–85 Ma), the magmatic foliation in the La Manaclá suite of hornblende gabbro-diorite-tonalite (89–83 Ma), the JBD zone (75–71 Ma), and the elongation of the lenticular bodies of sheared and pervasive serpentinized peridotites (Figure 1c; Escuder-Viruete, Valverde-Vaquero, Rojas-Agramonte, Gabites, & Pérez-Estaún, 2013). These characteristics suggest that the deformation in the shear zones is of Late Cretaceous age (Escuder-Viruete & Castillo-Carrión, 2016).

4. Mineral Chemistry

4.1. Major Elements

The major element composition of minerals was obtained by EMPA. Representative EMPA data of minerals, instrumental details and analytical conditions are given in Supporting Information S2 of the Data Repository (Escuder-Viruete et al., 2022). During the analysis, magmatic minerals were carefully distinguished from those recrystallized by metamorphic processes.

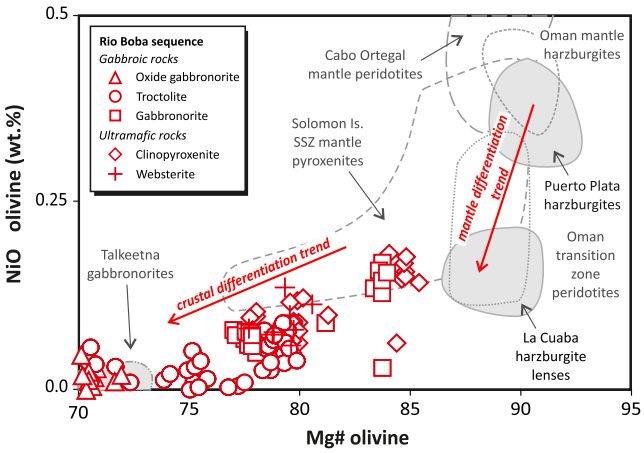

Figure 6. Olivine composition in the Rio Boba mafic-ultramafic plutonic sequence. Fields of olivine compositions: Omán mantle peridotites (Bodinier & Godard, 2007), Cabo Ortegal mantle peridotites (Santos et al., 2002), supra subduction zone mantle pyroxenites from Solomon Islands (Berly et al., 2006), and lower crustal gabbronorites in Talkeetna arc (Greene et al., 2006). Gray fields: olivine in Puerto Plata and La Cuaba harzburgites (Escuder-Viruete & Castillo-Carrión, 2016; Escuder-Viruete et al., 2014). Arrows reflect olivine differentiation trends in the Caribbean mantle and crustal rocks.

Olivine grains are compositionally unzoned and have the same composition in a given rock sample. In the pyroxenites, the Mg# values for olivine range from 77.8 to 85.4, with an average of 81.1 (Figure 6). In the gabbroic rocks, olivine has Mg# values of 77.1–83.8 (average 78.6) in the olivine gabbronorites, 69.7–79.9 (average 76.2) in the troctolites, and 69.8–72.1 (average 70.5) in the oxide gabbronorites. The Mg# versus NiO diagram (Figure 6) shows that olivine in some pyroxenites and gabbronorites has relatively high Mg# (~85) and NiO (0.15 wt.%), comparable to the olivine found in the SSZ mantle pyroxenites of Solomon Islands (Berly et al., 2006). These olivine compositions are close to the most evolved values on a mantle differentiation trend, along which Mg# and NiO both decrease, as defined in Figure 6 by the olivine compositions of the Puerto Plata and La Cuaba harzburgites of the Caribbean island arc (Escuder-Viruete & Castillo-Carrión, 2016; Escuder-Viruete et al., 2014). The mantle differentiation trend follows the compositional fields of olivine in the mantle peridotites of Oman (Bodinier & Godard, 2007) and the Cabo Ortegal (Santos et al., 2002). In contrast, the olivine in most of the pyroxenites and gabbroic rocks has significantly lower Mg# (~70–80) and NiO concentrations (<0.1 wt.%), comparable to olivine in the lower crustal gabbronorites of Talkeetna arc (Greene et al., 2006). These compositional relations indicate olivine crystallization from an already differentiated melt, following a crustal differentiation trend. The decrease of Mg# in olivine broadly reflect the crystallization of gabbronorites, troctolites and oxide gabbronorites as melts progressively evolve.

Spinel is rare in the pyroxenites. It is Cr and Al-rich [Cr# >0.5; Cr# = 100 × Cr/(Cr + Al)] in the clinopyroxenites and more Al-rich (Cr# <0.5) in part of the websterites. Spinels in the rest of websterites and gabbronorites are Mg-Al-rich hercynite, very poor in Cr (Cr# <0.05). The plastically deformed and recrystallized gabbronorites typically contain ilmenite grains, as well as exsolved ilmenite-magnetite pairs. TiO_2 contents in magnetite from these gabbronorites range between 5.2 and 3.0 wt.%.

Clinopyroxene has a relatively limited compositional variation, both in the pyroxenites and the gabbronorites. It ranges in composition from Al-Cr diopside to Al-Fe diopside and does not show systematic zoning in individual grains (Supporting Information S2). Clinopyroxene has Mg# values of 83.7–89.1 (average 86.0) in the clinopyroxenites and 85.9–89.6 (average 87.6) in the websterites. In the gabbroic rocks, clinopyroxene has Mg# values of 82.4–88.6 (average 85.0), 86.7–88.0 and 73.6–86.8 (average 79.2) in the gabbronorites, troctolites and oxide gabbronorites, respectively. Figure 7b shows that these Mg# values are lower than those of the clinopyroxene in the Puerto Plata and La Cuaba harburgites, SSZ (fore-arc) mantle peridotites and pyroxenites. However, clinopyroxene compositions in the Rio Boba sequence overlap those of the Solomon Islands mantle pyroxenites. In Figure 7b, the clinopyroxene define in each group of rocks a sub-parallel crustal fractionation trend, from high Mg# and low Al_2O_3 (1.6 wt.%) to lower Mg# and higher Al_2O_3 (3.6 wt.%), overlapping the compositional fields of arc-related crustal pyroxenites and mafic cumulates. The Cr_2O_3 contents range between 0.04 and 0.6 wt.% and are generally correlated with Mg#, with the exception of the oxide gabbronorites which have very low Cr_2O_3 (<0.1 wt.%). On the other hand, the clinopyroxenes have very low-Ti in all analyzed samples, particularly in the websterites and troctolites, similar to those of island arc cumulates and unlike the more TiO_2-rich clinopyroxene compositions of the ocean-ridge cumulates (Figure 7d). TiO_2 increasing up to 0.45 wt.%, with decreasing Mg#, also delineating a fractionation trend. This trend is followed at a lower Mg# by the composition of clinopyroxene in the mafic and intermediate lavas of the Puerca Gorda and Los Caños Formation.

In the TiO_2-Na_2O-SiO_2/100, ternary diagram of Figure 7a (Beccaluva et al., 1989), clinopyroxene compositions of the Rio Boba sequence are compared with the reference fields for diverse basaltic lavas in ophiolites as reported by Saccani and Photiades (2004). The clinopyroxenes of the pyroxenites, troctolites and gabbronorites plot in the fields of boninites, fore-arc basalts/basaltic andesites and IATs, while the clinopyroxenes of the oxide gabbronorites fall exclusively in the IAT field due to the relative larger content in Na_2O. In this diagram, clinopyroxene compositions from Puerca Gorda metavolcanic rocks and from Puerto Plata gabbroic rocks also display

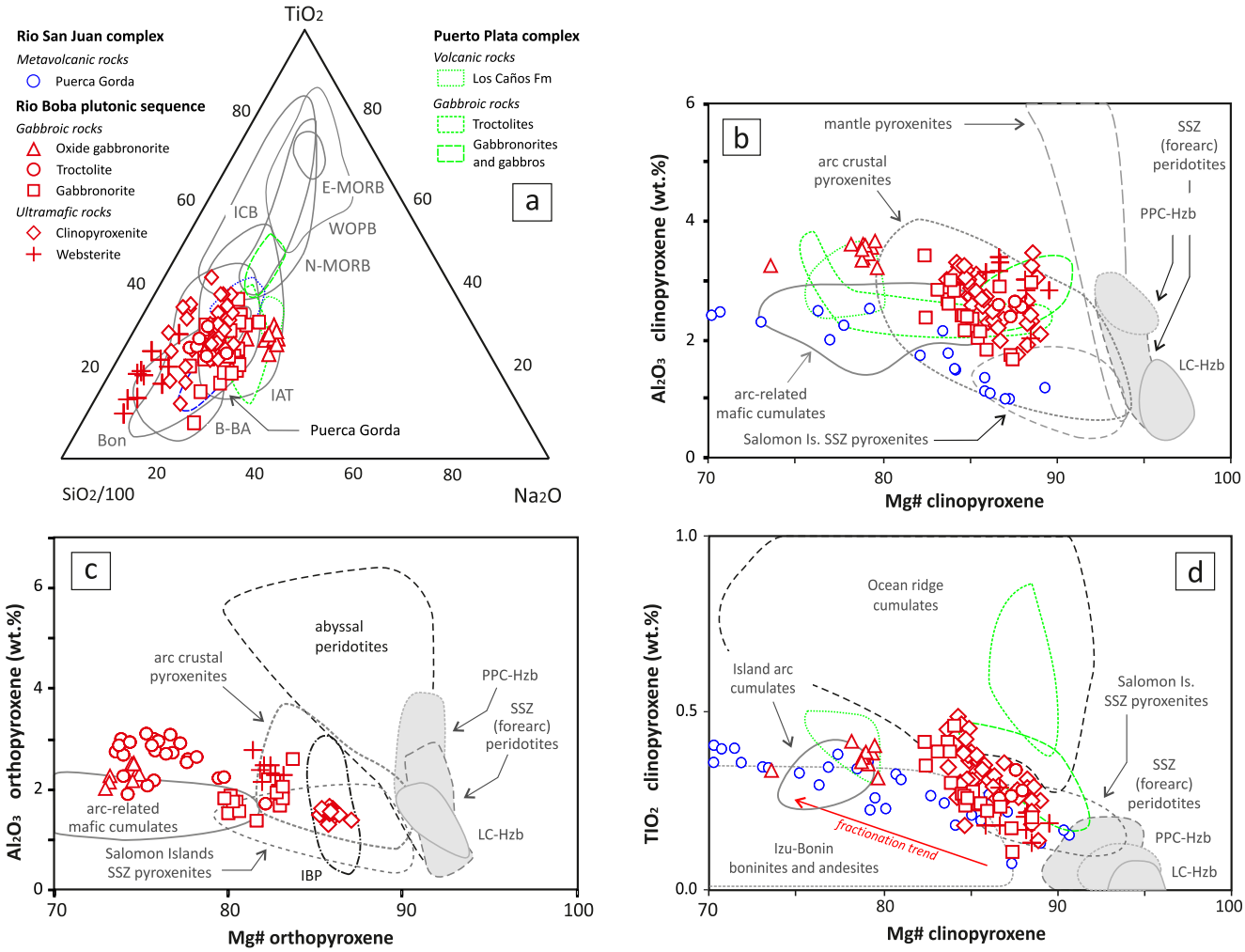

Figure 7. Pyroxene compositions in the Rio Boba mafic-ultramafic plutonic sequence. (a) TiO_2-Na_2O-SiO_2/100 (wt.%) discrimination diagram for clinopyroxene (Beccaluva et al., 1989). Fields representing clinopyroxene compositions in basalts from modern oceanic settings are reported for comparison (Saccani & Photiades, 2004). Abbreviations: N-MORB, normal MORB; E-MORB, enriched MORB; WOPB, within oceanic plate basalts; ICB, Iceland basalts; IAT, island arc tholeiites; Bon, boninites; B-BA, intra-oceanic fore-arc basalts and basaltic andesites. (b) Mg# versus Al_2O_3 (wt.%) for clinopyroxene. (c) Mg# versus Al_2O_3 (wt.%) for orthopyroxene. (d) Mg# versus TiO_2 (wt.%) for clinopyroxene. Fields for arc-related mantle pyroxenites, arc crustal pyroxenites, and arc-related mafic cumulates are from Berly et al. (2006) and references therein. Field for supra subduction zone (fore-arc) peridotites is from Bodinier and Godard (2007). Fields for ocean ridge cumulates and Izu-Bonin arc volcanic rocks are from Marchesi et al. (2006 and references therein). Compositions of Puerca Gorda mafic metavolcanic rocks and fields of Puerto Plata complex (PPC-Hzb) and La Cuaba harzburgites (LC-Hzb) are from Escuder-Viruete et al. (2014) and Escuder-Viruete and Castillo-Carrión (2016).

chemical compositions comparable to clinopyroxenes from boninitic basalts and intra-oceanic, fore-arc basalts/basaltic andesites.

Orthopyroxene compositions correlate with coexisting clinopyroxene compositions in a given plutonic rock type, but have slightly lower Al_2O_3 and slightly lower Mg# values (Figure 7c). In the clinopyroxenites, orthopyroxene has a narrow compositional range, with high Mg# of 85.2–87.0 (average 85.8) and low Al_2O_3 (1.36–1.54 wt.%), which is different of those from the abyssal and SSZ mantle peridotites. In the websterites, orthopyroxene have Mg# values of 81.2–82.1 and low Al_2O_3 of 2.1–2.79 wt.%. Orthopyroxene compositions from the pyroxenites plot in the fields of arc crustal pyroxenites and SSZ mantle pyroxenites of Solomon Islands (Figure 7c). Orthopyroxene has low Al_2O_3 (1.45–3.1 wt.%) and Mg# values of 73.6–82.1 (average 76.1) in the troctolites, 80.0–80.6 in the gabbronorites and 74.5–74.9 in the oxide gabbronorites. As in the case of clinopyroxene, the overall orthopyroxene compositions define a fractionation trend in which the Al_2O_3 slightly increases with decreasing Mg#, along the fields of arc crustal pyroxenites and arc-related mafic cumulates (Figure 7c). On the other hand, TiO_2 in the

orthopyroxene are very low, ranging from 0.08 to 0.16 wt.% in the pyroxenites to 0.02–0.18 wt.% in the gabbroic rocks. Cr_2O_3 is very low and range between 0.32 and 0.01 wt.%.

Plagioclase is an interstitial phase in the pyroxenites and the most abundant phase in the troctolites and gabbronorites. However, there is minimal intra-grain zoning or variation in anortite content (X_{An}). Measured X_{An} ranges between 0.90 and 0.98 in the pyroxenites, 0.94–0.99 in the troctolites, and 0.90–0.94 in the gabbronorites (Supporting Information S2). Some of the plagioclases analyzed in the gabbronorites show rims slightly more calcic than the cores.

4.2. Trace Elements in Clinopyroxene

In situ trace element analyses of magmatic clinopyroxene were carried out by LA-ICP-MS in 12 of the thick sections used for EMPA (three clinopyroxenites, two websterites, three troctolites, and four gabbronorites). Clinopyroxene analyzed in oxide gabbronorites showed evidence of metamorphic recrystallization and is not discussed here. Representative LA-ICP-MS data are given in Supporting Information S3. Chondrite-normalized (C) trace elements (REE) patterns of clinopyroxene in pyroxenites and gabbroic rocks of the Rio Boba plutonic sequence are displayed in Figure 8. In a first approximation, incompatible trace elements contents are very low in these rocks, with HREE absolute abundances between 1 and 8 times the chondrite value and sub-chondritic contents of high field strength elements (HFSE), particularly in Nb, Zr, Hf, and Ti. The shape of the trace elements patterns are similar, although the ranges of values vary from one group to another (see below). With the exception of clinopyroxenites, no zoning in REE composition has been detected between cores and rims of clinopyroxene grains.

The REE in the clinopyroxene of the clinopyroxenites are highly fractionated [$(La/Yb)_C$ = 0.16–0.53, average 0.26] and define convex-upward patterns (Figures 8a–8c). HREE concentrations are 2–5 times the chondrite values. In general, REE ratios increase from the core toward the rim of the individual grains. They show moderate to strong depletion of Nb, Zr and Hf relative to adjacent Th and LREE, and Ti relative to HREE. They lack a negative Eu anomaly, which could mean that the crystallization of clinopyroxene was not affected by plagioclase fractionation. Websterites present trace elements patterns very similar to clinopyroxenites, although they are distinguished by the extreme fractionation of REE [$(La/Yb)_C$ = 0.06–0.22, average 0.12] and a more pronounced anomaly in Zr-Hf (Figure 8d). HREE patterns are flat or shown a slight depletion [$(Sm/Yb)_C$ = 0.34–1.05, average 0.69]. The REE ratios in clinopyroxene from the Rio Boba pyroxenites are very similar to those in SSZ mantle clinopyroxenites and websterites from the Solomon Islands (Berly et al., 2006), as well as boninite-type mafic-ultramafic cumulates from northern Victoria Land (Tribuzio et al., 2008).

The REE ratios in the clinopyroxene of the gabbronorites are also very fractionated [$(La/Yb)_C$ = 0.06–0.28, average 0.14]. HREE ratios are 3–8 times chondrite value, showing convex-upward trace elements patterns with strongly fractionated LREE and flat HREE segments (Figures 8f and 8g). These patterns exhibit prominent negative anomalies in Nb, Zr, and Ti, and lack any Eu anomaly. Overall, clinopyroxene trace element patterns in the gabbronorites are subparallel to those of the pyroxenites but located at slight higher values. These trace elements patterns are subparallel and have REE ratios similar to those of the clinopyroxenes from the mafic-ultramafic boninitic cumulates, the Puerca Gorda metabasalts and the gabbroic rocks of the Puerto Plata SSZ ophiolitic complex (Escuder-Viruete, Friedman, et al., 2011; Escuder-Viruete et al., 2014).

The clinopyroxene from the troctolites also show trace elements patterns with very low HREE concentrations, 6–8 times the chondrite value, below N-MORB. These patterns are strongly fractionated [$(La/Yb)_C$ = 0.10–0.12] with a slightly convex-upward shape and flat HREE segments (Figure 8e). They are characterized by depletion of Zr and Hf relative to Th and LREE, and a Ti negative anomaly relative to HREE, but lack a Nb and Eu anomalies. As in gabbronorites, the Th values are relatively high and the HREE ratios are 4–8 times higher than in the pyroxenites. These clinopyroxenes show trace elements patterns similar to those in mafic-ultramafic boninitic cumulates and layered troctolites of boninitic affinity of the Puerto Plata ophiolite complex.

For comparison, the trace elements contents of clinopyroxene in metapicrites and high-Mg metabasalts of the Puerca Gorda Schists are displayed in Figure 8h. The incompatible trace elements ratios are low and vary between 0.4 and 9.6 times the chondrite value, below N-MORB. The REE values are variably fractionated ($[La/Yb]_c$ = 0.5–1.8; average 0.8). All trace element patterns are flat to slightly convex-upward and show depletion of Nb, Zr and Hf relative to Th and LREE, and Ti depletion relative to HREE. In general, crystal rims shows

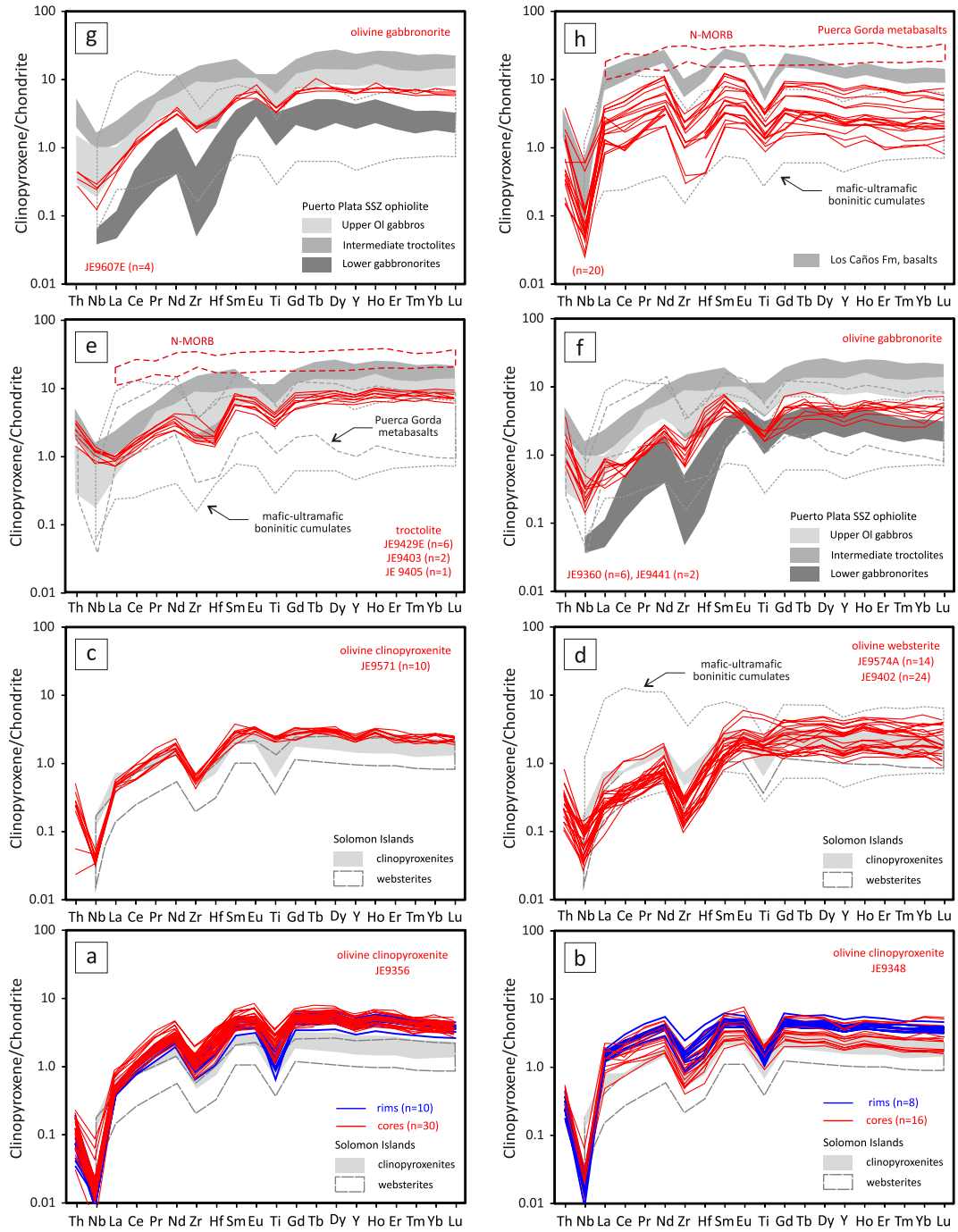

Figure 8. Representative chondrite-normalized (chondrite values, Sun & McDonough, 1989) trace element patterns for clinopyroxene in the Rio Boba mafic-ultramafic plutonic sequence: (a–c) olivine clinopyroxenite; (d) olivine websterite; (e) troctolite; and (f and h) olivine gabbronorite. (g) Puerca Gorda metabasalts. Fields of clinopyroxene in supra subduction zone mantle clinopyroxenites and websterites of the Solomon Islands are from Berly et al. (2006). Clinopyroxene in gabbroic and Los Caños volcanic rocks from Puerto Plata ophiolitic complex and in metapicrites and high-Mg metabasalts of the Puerca Gorda Schists are from Escuder-Viruete, Friedman, et al. (2011) and Escuder-Viruete et al. (2014). See text for explanation.

higher trace element values than the crystal cores. Crystal cores and rims lack a negative Eu anomaly, which could mean that the crystallization of clinopyroxene was not affected by plagioclase fractionation. These trace elements patterns are analogous to those of clinopyroxenes from the mafic-ultramafic boninitic cumulates and basalts of Los Caños Fm of the Puerto Plata ophiolite complex.

5. Whole-Rock Geochemistry

5.1. Chemical Changes Due To Alteration and Metamorphism

Whole-rock compositions of major and trace elements were obtained by ICP-MS analysis of powdered samples fused with $LiBO_2$. For a subset of samples, whole-rock Th, Nb, Ta, La, Pb, Nd, Sm, Zr, and Hf were also analyzed by high resolution ICP-MS with high-pressure dissolution and HF–HNO_3 digestion. Results are reported in Supporting Information S4, as well as details of analytical techniques, including accuracy and precision. In occasions, the ultramafic and gabbroic rocks of the Rio Boba sequence have been heterogeneously deformed and metamorphosed to granulite, amphibolite, and greenschists facies conditions. Therefore, the mobility during metamorphism of certain major (e.g., Si, Na, K, and Ca) and trace (e.g., B, Li, Cs, Rb, Ba, U, and Sr) elements may have modified the primary whole-rock geochemistry. However, the HFSE (Nb, Ta, Zr, Hf, Ti, and Y), REE, transition elements (V, Cr, Ni, and Sc), and Th, generally remain unaffected at the scale of hand-specimen under a wide range of metamorphic conditions (e.g., Bédard, 1999; Pearce & Peate, 1995). Accordingly, the following geochemical characterization of rock samples, calculation of equilibrium melts and petrogenetic discussion will be based mostly on the HFSE and REE.

5.2. Major Elements

Major elements in ultramafic and gabbroic rocks are plotted and compared with reference compositional fields in the variation diagrams of Figure 9. These reference fields correspond to: the upper crustal mafic metavolcanic rocks of the Puerca Gorda Schists; primitive (Mg# >66) low-, intermediate-, and high-Ca boninites from the ODP Leg 125 (Crawford et al., 1989; Pearce & Peate, 1995; Pearce et al., 1992; Taylor et al., 1994); plutonic rocks from the Early to Middle Jurassic Talkeetna Arc section (Greene et al., 2006); SSZ mantle pyroxenites of Solomon Islands (Berly et al., 2006); and the experimentally obtained liquid line of descent of anhydrous, mantle derived, tholeiitic liquids by fractional crystallization at 0.7 and 1.0 GPa (Villiger et al., 2004, 2007).

The clinopyroxenites and websterites display high Mg# values of 77–86 [Mg# = Mg/(Mg + Fe) × 100, calculated as cation wt.%] for a wide range in the Al_2O_3, FeO_T and CaO contents. In comparison, the gabbroic rocks show a smaller range and define a more regular trend with Mg# values of 64–81 in the gabbronorites, 65–79 in the troctolites, and 42–66 in the oxide gabbronorites. Therefore, if we consider the decreasing Mg# as an indicator of the degree of magmatic fractionation, there is a clear order from the most primitive compositions of the clinopyroxenites and websterites, to the more evolved gabbronorites, troctolites and oxide gabbronorites. The <70 Mg# values in many gabbroic rocks indicate that they are already evolved melts, and are out of equilibrium with upper mantle peridotite (Müntener & Ulmer, 2018). However, these pyroxenites and gabbroic rocks display cumulate textures, products of solid-liquid separation processes. Therefore, their whole-rock compositions are strongly controlled by the cumulate phases. Thus, they do not likely represent liquid compositions.

As the Mg# decreases, Al_2O_3 and CaO first define a rapid increase in the pyroxenites (Al_2O_3 from 4.7 to 14.0 wt.%), followed by a regular decrease in the gabbroic rocks (Al_2O_3 from 22 to 16 wt.%), with a minimal compositional overlap between gabbronorites and oxide gabbronorites. This change in trend of Al_2O_3 and CaO coincides with the initiation of plagioclase crystallization. These rocks, however, have an obvious plagioclase cumulate component and their compositions are therefore strongly controlled by the cumulate phases. This compositional effect due to plagioclase crystallization and cumulate formation matches the lower Al_2O_3 and CaO contents of the mafic volcanic rocks of Puerca Gorda Schists, which for similar Mg# values do not commonly contain abundant phenocrysts. This suggests that these volcanic rocks are the extrusive equivalents of the liquids in equilibrium with the cumulates (see below).

The degree of magmatic fractionation is also expressed with the progressive increase in TiO_2 and FeO_T with decreasing Mg#. However, all the studied samples have very low TiO_2, in particular pyroxenites (0.10–0.24 wt.%), troctolites (<0.1 wt.%) and olivine gabbronorites (0.03–1.21 wt.%), which are similar to those of the mafic metavolcanic rocks of the Puerca Gorda and the primitive boninites of the ODP Leg 125. The relatively higher TiO_2 of oxide gabbronorites may be due to the accumulation of Fe-Ti oxides in these more evolved magmas.

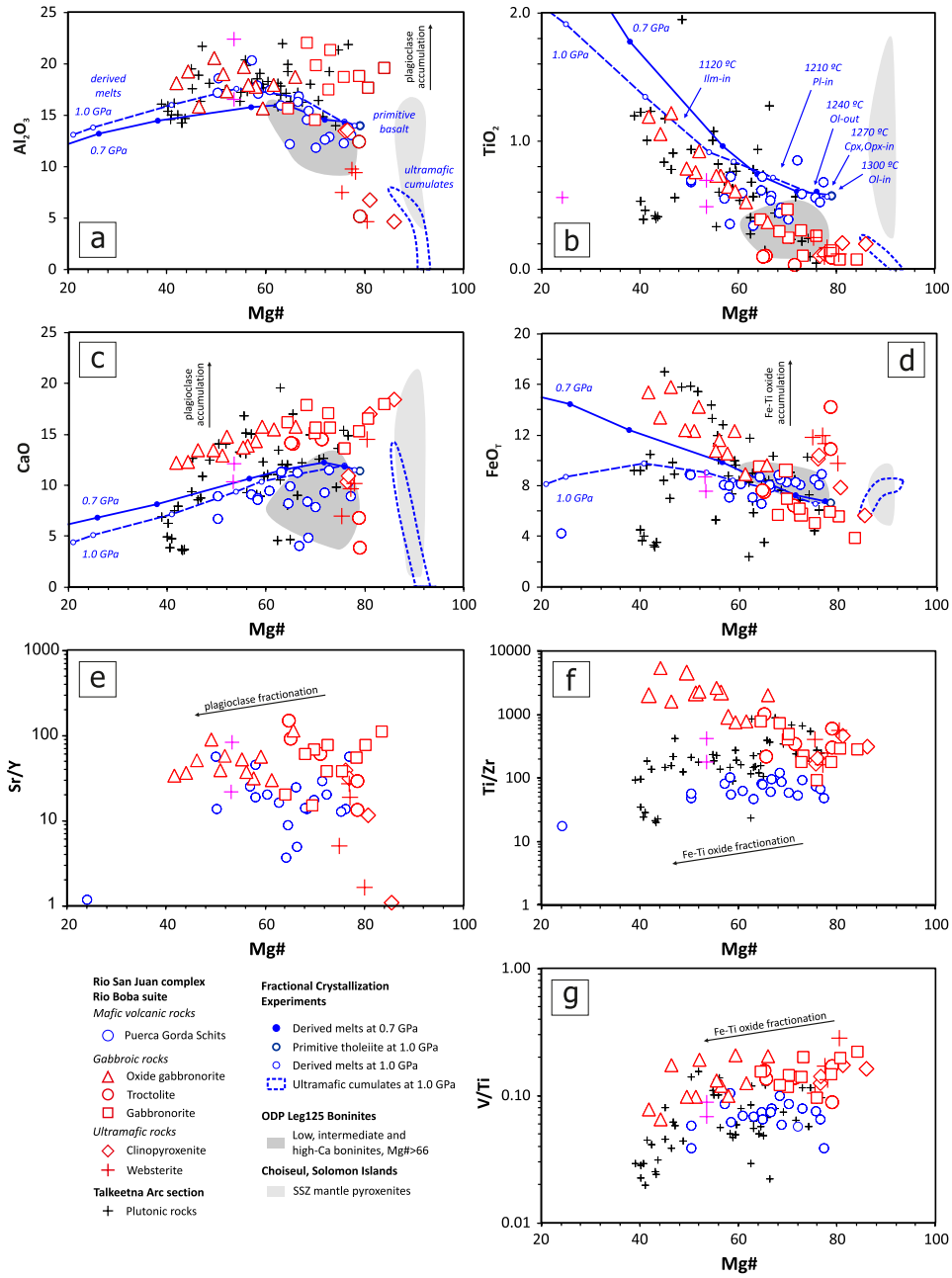

Figure 9. Mg# versus Al_2O_3 (a), TiO_2 (b), CaO (c), FeO_T (d), Sr/Y (e), Ti/Zr (f), and V/Ti (g) variation diagrams for mafic and ultramafic rocks of the Rio Boba plutonic sequence and mafic metavolcanic rocks of the Puerca Gorda Schists (see also Escuder-Viruete, Friedman, et al., 2011). All data on anhydrous basis in wt.%. Gray and light gray fields correspond to low-, intermediate-, and high-Ca boninites from the ODP Leg 125 (Crawford et al., 1989; Pearce & Peate, 1995; Pearce et al., 1992; Taylor et al., 1994) and supra subduction zone mantle pyroxenites of Solomon Islands (Berly et al., 2006). Plutonic rocks from the Early to Middle Jurassic Talkeetna Arc section (Greene et al., 2006) are plotted for comparisons with a well-documented arc crustal sequence analog. Blue points and lines join melts obtained experimentally for the fractional crystallization of anhydrous, mantle derived, tholeiitic melts at 0.7 and 1.0 GPa (liquid lines of descent from Villiger et al. (2004, 2007)). See text for explanation.

Overall, the major element composition of the gabbronorites is similar to the Talkeetna Arc rocks, though some of the more evolved Talkeetna samples have lower CaO, TiO_2, and FeO_T for similar Mg#. The pyroxenites display a restricted compositional range and can be compared with the pyroxenites of the Solomon Islands, although they have a lower Mg# (Figure 9).

The experimental models for anhydrous fractional crystallization of primitive tholeiitic basalt at the base of the crust (1.0 GPa) and at shallower crustal conditions (0.7 GPa) show a continuous differentiation trend from high Mg# cumulates (dunite, lherzolite and websterite) to evolved, low Mg# liquids (dots and lines in Figure 9). Gabbroic samples plot following a trend subparallel to the experimental liquid line of descent in the Mg# 80–40 interval. This trend is continuous with no gaps in Mg#. The Rio Boba gabbroic rocks plot away from the experimental crystallization lines at 0.7 and 1.0 Gpa in the CaO, TiO_2, and FeO_T versus Mg# diagrams, reflecting a variability that may be related to fractional crystallization. These differences may be due to a different starting basalt composition and/or the elimination of all solid phases in each single fractionation step and/or the constant pressure conditions followed in the modeling (see Villiger et al., 2004, 2007). With some exception, the dunite-wehrlite-pyroxenite cumulates obtained in the modeling of anhydrous fractional crystallization have higher Mg# values than the Rio Boba pyroxenites, suggesting that these pyroxenites are products of the crystallization of already evolved mantle-derived magmas. This is consistent with the lower Mg# values with respect to the SSZ mantle pyroxenites of the Solomon Islands.

The concentrations of Cr, Ni, V, and Sc are higher in pyroxenites and progressively decrease from the gabbronorites to the oxide gabbronorites (Supporting Information S4). The concentrations of these elements in the Puerca Gorda mafic metavolcanic rocks are similar to those in the gabbronorites. With some exception of the more evolved oxides gabbronorites, the mafic plutonic rocks of the Rio Boba sequence and the metavolcanic rocks of Puerca Gorda have Ti/V values equal to, and lower than, chondrite (<10), which values are similar to those of the boninites, suggesting high depletion in the mantle source. Zr concentration shows an incompatible behavior increasing from very low levels in the pyroxenites and gabbronorites to higher concentrations in the mafic metavolcanic rocks.

5.3. Trace Elements

The pyroxenites and gabbroic rocks are highly depleted in terms of REE and other trace elements, having concentrations lower than those of N-MORB and in some cases below 0.1 times N-MORB (Supporting Information S4). Overall, REE values (ΣREE) systematically increase as follows: clinopyroxenites and websterites (3.2–9.0), to olivine gabbronorites (2.8–5.8), troctolites (2.0–8.8), gabbronorites (4.2–16.3), and oxide gabbronorites (4.3–16.7). In the N-MORB (N) normalized diagrams of Figure 10, all samples show remarkably parallel trace element patterns. They are characterized by an enrichment in LILE (Rb, Ba, K, Pb, and Sr, but generally no Th) relative to the HREE, Ti and Y, and have high fluid mobile/immobile element ratios (i.e., Ba/La, Sr/Nd, and Pb/Ce <<1). Such features are commonly attributed to an aqueous fluid component in the source (Pearce & Peate, 1995). The patterns also show pronounced negative anomalies in HFSE (i.e., Ta, Nb, Zr, and Hf) which are typical of subduction-related magmas (Pearce & Peate, 1995). It should be noted that the lack of correlation between LILE contents and the loss on ignition (not shown) suggest that metamorphism and low-T alteration did not influenced the trace element abundances of these rocks.

In the N-MORB normalized diagrams (Figure 10a), the clinopyroxenites and websterites shown generally a LREE depletion ($0.10 < La_N/Nd_N < 1.12$) and flat HREE segments ($0.60 < Sm_N/Yb_N < 0.97$). Pyroxenites do not present a clear Eu anomaly [Eu* = 0.88–1.42, where $Eu^* = (Eu_C/(Sm_C + Gd_C)0.5)$]. The troctolites also display a LREE depletion ($0.12 < La_N/Nd_N < 1.02$) and a sub-horizontal to moderate HREE depletion ($0.75 < Sm_N/Yb_N < 2.92$). These rocks exhibit a moderate to pronounced positive Eu anomaly (Eu/Eu* = 1.48–2.15), reflecting their plagioclase-cumulate nature. Compositionally, they are comparable to the intermediate troctolites of the Puerto Plata complex (Figure 10b). The gabbronorites have a pronounced LREE depletion ($0.18 < La_N/Nd_N < 0.54$) and a flat to slight HREE depletion ($0.72 < Sm_N/Yb_N < 1.4$). The pronounced LREE depletion ($0.19 < La_N/Nd_N < 0.72$) and the flat HREE segment ($0.87 < Sm_N/Yb_N < 1.18$) is also characteristic of the trace element patterns of the oxide gabbronorites. Gabbronorites and oxide gabbronorites present a moderate Eu anomaly (Eu/Eu* = 1.17–1.66 and 1.18–2.03, respectively) indicative of plagioclase accumulation. Compositionally, the gabbronorites of the Rio Boba sequence are comparable to the lower and upper gabbronorites of the Puerto Plata complex, as well as the more primitive plutonic rocks of the Talkeetna Arc (Figures 10c, 10d). The Ti anomaly relative to HREE is slightly negative in the pyroxenites, troctolites and gabbronorites. However,

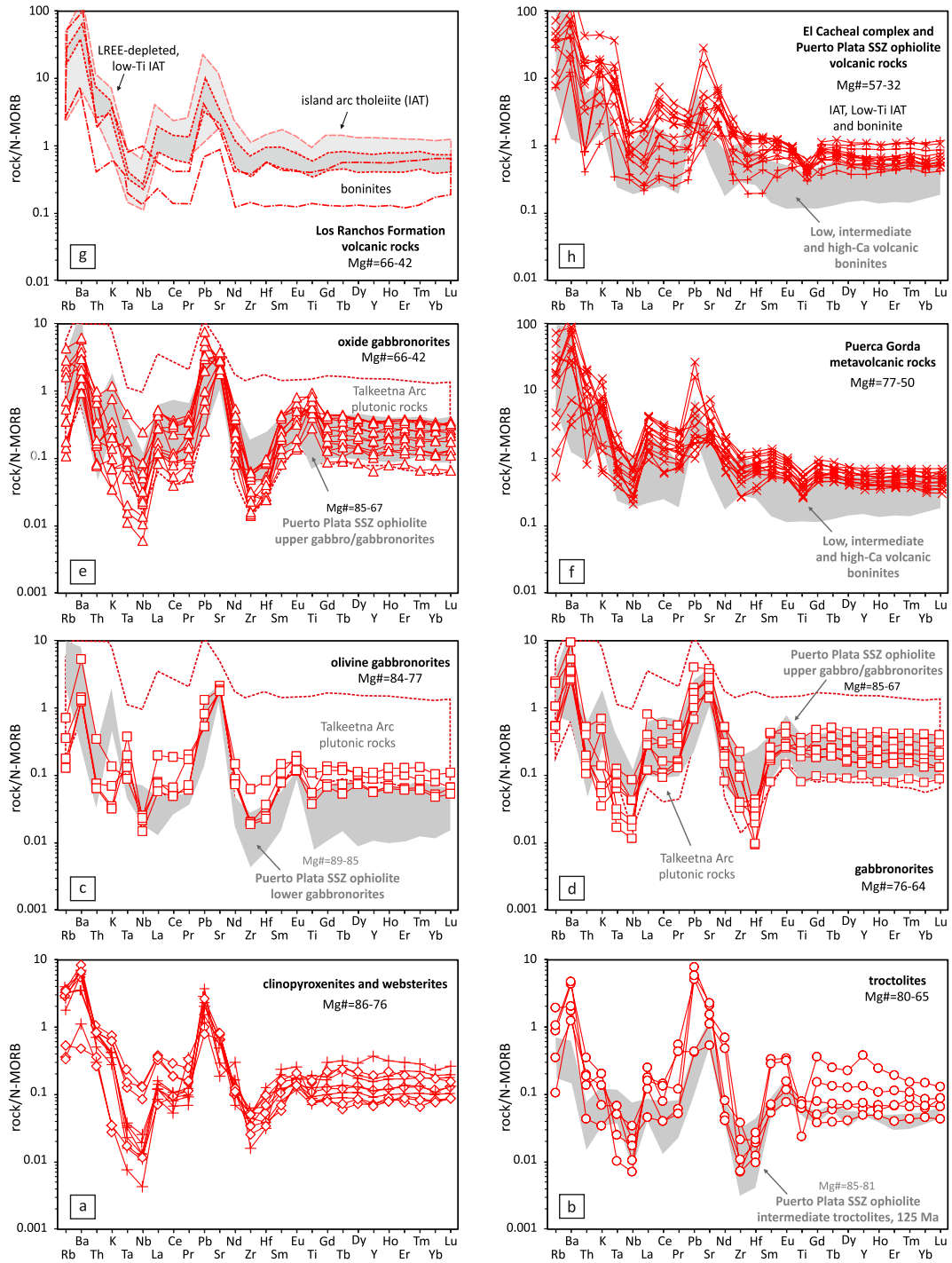

Figure 10. N-MORB-normalized trace-element plots for mafic and ultramafic rocks of the Rio Boba plutonic sequence, as well as for other regionally related volcanic rocks. (a) Pyroxenites, (b) troctolites, (c) olivine gabbronorites, (d) gabbronorites, (e) oxide gabbronorites, (f) Puerca Gorda Schists, (g) main geochemical groups of Lower Cretaceous volcanic rocks in Hispaniola, and (h) mafic volcanic rocks from El Cacheal complex and Los Caños Fm of Puerto Plata ophiolitic complex (data from Escuder-Viruete, Friedman, et al., 2011; Escuder-Viruete et al., 2006, 2014, and this work). MORB-normalizing values are from Sun and McDonough (1989). Boninite compositions are from the ODP Leg 125 (Pearce & Peate, 1995; Pearce & Reagan, 2019; Pearce et al., 1992; Taylor et al., 1994). See text for explanation.

the evolved oxide gabbronorites show a marked positive Ti anomaly, related to the late crystallization of Fe-Ti oxides (Figure 10e). Given the high Mg#, the significant LREE depletion, very low TiO_2 concentrations and low HREE values, indicate a strongly depleted mantle source for both pyroxenites and gabbroic rocks of the Rio Boba sequence and/or high-degrees of partial melting.

The trace element compositions of the Puerca Gorda mafic metavolcanic rocks were reported by Escuder-Viruete, Friedman, et al. (2011). Their patterns are characterized by a moderate to strong LREE enrichment ($1.5 < La_N/Nd_N < 2.2$) and HREE depletion ($1.2 < Sm_N/Yb_N < 2.4$; Figure 10f). These metavolcanic rocks show a prominent negative Ti anomaly, but they lack an Eu anomaly (Eu/Eu* = 0.90–1.12). The LREE depletion, low-TiO_2, and lower Ti/V values, as well as lower HREE levels, suggest that the source for these rocks was strongly depleted mantle and/or the protoliths were affected by high degrees of partial melting. Their trace element patterns are comparable to low-Ti IAT and boninites of the Lower Cretaceous Puerto Plata (Los Caños Fm) and El Cacheal complexes (Figure 10h; Escuder-Viruete et al., 2014), as well as boninites from the Marianas, New Caledonia and Izu-Bonin fore-arc (Pearce & Peate, 1995; Pearce & Reagan, 2019).

6. Discussion

6.1. Formation of the Plutonic Sequence by Fractional Crystallization

The mafic and ultramafic rocks of the Rio Boba plutonic sequence exhibit textures varying from adcumulate to orthocumulate. The cumulate textures are the product of solid-liquid separation processes, evidenced by modal and grain-size layering from decimeter to millimeter scale. Cumulate textures imply fractional crystallization in a magmatic system as the main differentiation process. In this situation, it is not surprising that the variation in the whole-rock major and trace-element composition of the rock is controlled by the cumulate phases.

Plagioclase is the dominant phase in the cumulate gabbronorites. The whole-rock Al_2O_3 and CaO contents are the result of plagioclase fractionation. The variable, but always present, positive Eu anomaly clearly reflects the cumulate nature of the gabbronorites and troctolites. The absence of a clear positive Eu anomaly in the pyroxenites suggests that plagioclase was not present in the primary melt in equilibrium with the residual mantle. Also, the absence of a Eu anomaly in the related Puerca Gorda volcanic rocks indicates that plagioclase accumulation processes did not affect them, which is consistent with the absence of plagioclase phenocrysts. The effects of the plagioclase fractionation can be visualized with the help of diagrams of whole-rock trace elements ratios. In Figure 9, the trend in Sr/Y appears generally to be the result of plagioclase fractionation in the cumulate gabbronorites and in the more evolved oxide gabbronorites, analogously to the Sr/Y trend described in the Talkeetna arc (Greene et al., 2006). The diagram also shows that for a similar value of Mg#, the Sr/Y ratio is generally higher due to the plagioclase accumulation in gabbroic rocks than in Puerca Gorda mafic volcanic rocks, which magmatic evolution was not primary controlled by the fractionation of this mineral.

Fe-Ti oxides (magnetite-ilmenite) are also major phases in the gabbroic rocks and their crystallization largely controlled the whole-rock FeO_T and TiO_2 of the oxide gabbronorites and related mafic volcanic rocks. This is particularly evident in the trace-element patterns of Figure 10, where the oxide gabbronorite samples have pronounced positive Ti anomalies, and the mafic volcanic rocks of Puerca Gorda exhibit complementary negative Ti anomalies. Although the parent magma was probably depleted in Ti relative to HREE in the source, the crystallization of Fe-Ti oxides within the gabbronorites and particularly in the oxide gabbronorites gave rise to magmas depleted in TiO_2 that formed the volcanic sequence. In Figure 9, the crystallization of V-rich, Fe-Ti oxides in the gabbronorites is reflected by a trend of increasing Ti/Zr and decreasing V/Ti from the more primitive gabbronorites to the more evolved oxide gabbronorites. As Zr appears to be controlled almost exclusively by fractionation, increasing of the Ti/Zr ratio monitors the Fe-Ti oxide accumulation in the oxide gabbronorites, which does not take place in volcanic rocks. The trends of variation in Ti/Zr and V/Ti in the gabbroic rocks of Rio Boba are also recorded in the plutonic and volcanic rocks of Talkeetna arc section (Figure 9), which have been interpreted by Greene et al. (2006) as a strong signature of Fe-Ti oxide fractionation.

6.2. Experimental Constraints on Parental Melt, Phase Crystallization Sequence, Pressure Conditions, and Water Content

Experimental studies indicate that fractional crystallization of anhydrous, mantle derived, tholeiitic liquids in the temperature range of 1,060°C–1,330°C at 0.7 GPa (lower crust conditions) and 1.0 GPa (base of the arc crust conditions) produces phase relations in proportions and compositions that explain the characteristics of ultramafic to mafic lower crustal cumulate rocks (Müntener & Ulmer, 2018; Müntener et al., 2001; Villiger et al., 2004, 2007). Although, the temperature of first appearance of each phase varies for each phase assemblage, the crystallization sequence is similar at 0.7 and 1.0 GPa. With falling temperature in the experimental run (Figure 9), the crystallization sequence begins with olivine and spinel as liquidus phases at 1,300°C and continues with the appearance of olivine, spinel, clino and orthopyroxene, until the disappearance of olivine at 1,240°C. The first appearance of plagioclase is at 1,210°C at both 0.7 and 1.0 GPa, coprecipitating with spinel, clinopyroxene and ortopyroxene. Between 1,210°C and 1,180°C, plagioclase and spinel crystallize (orthopyroxene-out). At 1,060°C the stable assemblage is clinopyroxene, plagioclase and ilmenite (±quartz). This crystallization sequence is controlled by the peritectic reaction olivine + liquid = orthopyroxene and the early plagioclase saturation (e.g., Müntener et al., 2001).

Therefore, the experimentally obtained crystallization sequence for anhydrous tholeiitic melts explains the association of mafic and ultramafic rocks in the Rio Boba plutonic sequence, where the pyroxene crystallization precedes plagioclase crystallization. In this sense, the modal compositions, mineral chemistry and whole-rock compositions of the Rio Boba pyroxenites and gabbroic rocks represent a cumulate sequence formed by fractionation of tholeiitic magmas with very low initial H_2O in the lower crust of the arc. Melts evolved along the simplified crystallization sequence of olivine → pyroxenes → plagioclase → Fe-Ti oxides (±quartz).

Several arguments support the formation of the Rio Boba plutonic rocks following this crystallization sequence. (a) Mg# and NiO in olivine decrease progressively from the pyroxenites and troctolites to the olivine gabbronorites and oxide gabbronorites. (b) The decrease in Mg# and the increase in Al_2O_3 and TiO_2 in the orthopyroxene and clinopyroxene are negatively correlated from the pyroxenites to gabbronorites and oxide gabbronorites. (c) The Mg# decrease in the spinel, which varies in composition from Cr-rich spinel to hercynite, culminating in Fe-Ti oxides in the most evolved rocks. (d) Anorthite-rich, anhedral plagioclase occurs between cumulus olivine and pyroxenes in the pyroxenites, which is attributed to the entrapment of melt among cumulus phases. (e) The crystallization (and accumulation) of the successive mineral phases of the sequence exerts a control on the variation of the whole-rock major-element compositions (Al_2O_3, CaO, FeO_T, and TiO_2). (f) The incompatible trace elements concentrations (e.g., Th, HFSE, and REE) increase with the decrease in Mg#, both in clinopyroxene and in whole-rock, from the clinopyroxenites and websterites to troctolites and gabbronorites (as well as the related Puerca Gorda volcanic rocks). (g) The magmatic amphibole is very scarce or absent, appearing only as a late magmatic phase.

For these reasons, we propose that the Rio Boba plutonic sequence is of cumulus origin and was controlled by fractional crystallization (and post-cumulus melt entrapment), as follows. The initial precipitation of olivine and Cr-rich spinel was followed by the crystallization of clinopyroxene and orthopyroxene, giving rise to olivine clinopyroxenite and websterite cumulates. Residual melts evolved through a fractional crystallization, initially controlled by olivine separation, which led to the formation of olivine-free websterites. Subsequent melts were controlled by the crystallization of An-rich plagioclase, and clinopyroxene, resulting in the development of the gabbronorites. The crystallization of Fe-Ti oxide also plays a major role in the late-stage fractional crystallization process and gave rise to the oxide gabbronorite. Accordingly, the absence of magmatic amphibole and garnet in the crystallization sequence implies a very low initial H_2O content in the magma (e.g., Alonso-Perez et al., 2009), and constraints the formation of the cumulate sequence to intermediate pressures typical of the lower arc crust (<1.0 GPa; Jagoutz et al., 2011). However, the Rio Boba troctolites recorded a crystallization sequence in which the crystallization of olivine and plagioclase precedes that of pyroxene. Therefore, although volumetrically less important, troctolitic gabbros represent a distinctive cumulate sequence formed by fractionation of anhydrous tholeiitic magmas at lower pressures (<0.45 GPa; Villiger et al., 2007).

6.3. Petrogenetic Relationships Between Plutonic and Volcanic Rocks

Establishing petrogenetic relationships between the Rio Boba plutonic sequence and the spatially related Puerca Gorda volcanic rocks are key to establish the nature of the mantle source of the magmas and to reconstruct the crustal section of the intra-oceanic Caribbean island arc. Field, petrographic and geochemical data described above provide strong evidence that the cumulate pyroxenites and gabbronorites are the product of partial crystallization of a magma whose remaining liquid was subsequently removed. A reasonable hypothesis is that this remnant liquid erupted as the volcanic rocks that make up the upper arc crust. This possibility can be tested by checking whether the cumulate pyroxenites and gabbronorites crystallized in equilibrium with liquids compositionally similar to the Puerca Gorda volcanic rocks and other regional volcanic units of the Caribbean island arc.

For this purpose, the composition of the "equilibrium melts" was calculated using the trace-element composition of magmatic clinopyroxene in selected pyroxenites and gabbronorites, and appropriate clinopyroxene/melt partition coefficients (e.g., Bédard, 2005). Clinopyroxenes with petrographic evidence of deformation or recrystallization were not used in the calculation of equilibrium melts, since it may have changed the composition during metamorphic re-equilibrium at high-T. Further uncertainties in the equilibrium melt composition are due to the fact that clinopyroxene could have formed from a melt trapped in the interstices of cumulus minerals. In this case, the post-cumulus clinopyroxene may yield anomalously high concentration of incompatible elements due to closed-system crystallization (e.g., Bédard, 1999). In the analyzed clinopyroxenes, this effect is revealed by relatively high concentrations of HFSE and HREE. To avoid this effect, the samples selected in this study have a high clinopyroxene modal content and, in each sample, several large (0.2–10 mm) cumulus clinopyroxenes were analyzed. At thin section scale, no significant grain-to-grain variation in the incompatible elements composition of clinopyroxene was detected, suggesting that post-cumulus processes did not significantly affect its trace element characteristics. Calculated equilibrium melts are reported in Supporting Information S5 and plotted in the chondrite-normalized trace elements diagrams of Figure 11.

The melts modeled in equilibrium with the clinopyroxenites and websterites have low TiO_2, HFSE and REE contents, where the HREE ratios are only 2–10 times chondrite. Their patterns show variable LREE depletion and pronounced Nb and Zr-Hf negative anomalies (Figures 11a–11c). These characteristics are indicative of a strongly depleted mantle source and/or they result from high degrees of partial melting, with a variable, but generally small, subduction fluid component. Model melts are compositionally similar to the boninite and low-Ti IAT protoliths of the Puerca Gorda Schists, supporting a genetic relationship through crystal fractionation processes. They also show compositional affinities with the LREE-depleted IAT volcanic rocks of the Cacheal complex and Los Ranchos Fm, and the melts in equilibrium with the lower gabbronorites of the Puerto Plata complex. The model shows that melts in equilibrium with olivine websterite are similar to representative intermediate and high-Ca boninite lavas (Figure 11c), suggesting that these cumulates derived from boninite-like magmas. Crawford et al. (1989) and Fallow and Crawford (1991) describe primitive high Ca boninite lavas with phenocrysts of olivine, orthopyroxene and clinopyroxene, which correspond to the cumulus phases found in the olivine clinopyroxenites and websterites.

The melts modeled in equilibrium with gabbronorites show a flat trace elements pattern with a strong positive Th and negative Zr-Hf and Ti anomalies (Figure 11d). The LREE are generally slightly depleted and HREE absolute abundances are low (5–10 times chondrite), which also point to a depleted mantle source modified by a small component of subduction-related fluid. These model melts are similar to the low-Ti IAT and boninitic protoliths of Puerca Gorda Schists, the lavas of the Los Ranchos Formation, and melts in equilibrium with upper gabbronorites of the Puerto Plata complex. This suggests that the gabbronorites crystallized in equilibrium with melts that were extracted and erupted to produce these volcanic rocks (Figure 11d). Crawford et al. (1989) describe evolved high-Ca boninite lavas with plagioclase phenocrysts associated with clinopyroxene, olivine and orthopyroxene, which correspond to the cumulus phases in the gabbronorites.

Although few data are available, the model of the melts in equilibrium with the troctolites also has low Ti contents and HREE absolute abundances (about 10 times chondrite), suggesting, as in the case of the pyroxenites, a depleted mantle source (Figure 11e). However, model liquids show a distinctive flat trace elements pattern, with relatively high Th and Nb, indicating an additional melt component in the source, such as partial melted subducted sediments (Hochstaedter et al., 2001; Tollstrup et al., 2010). These modeled melts in equilibrium with the troctolite cumulate are compositionally similar to the boninite protoliths of the Puerca Gorda Schists and melts in

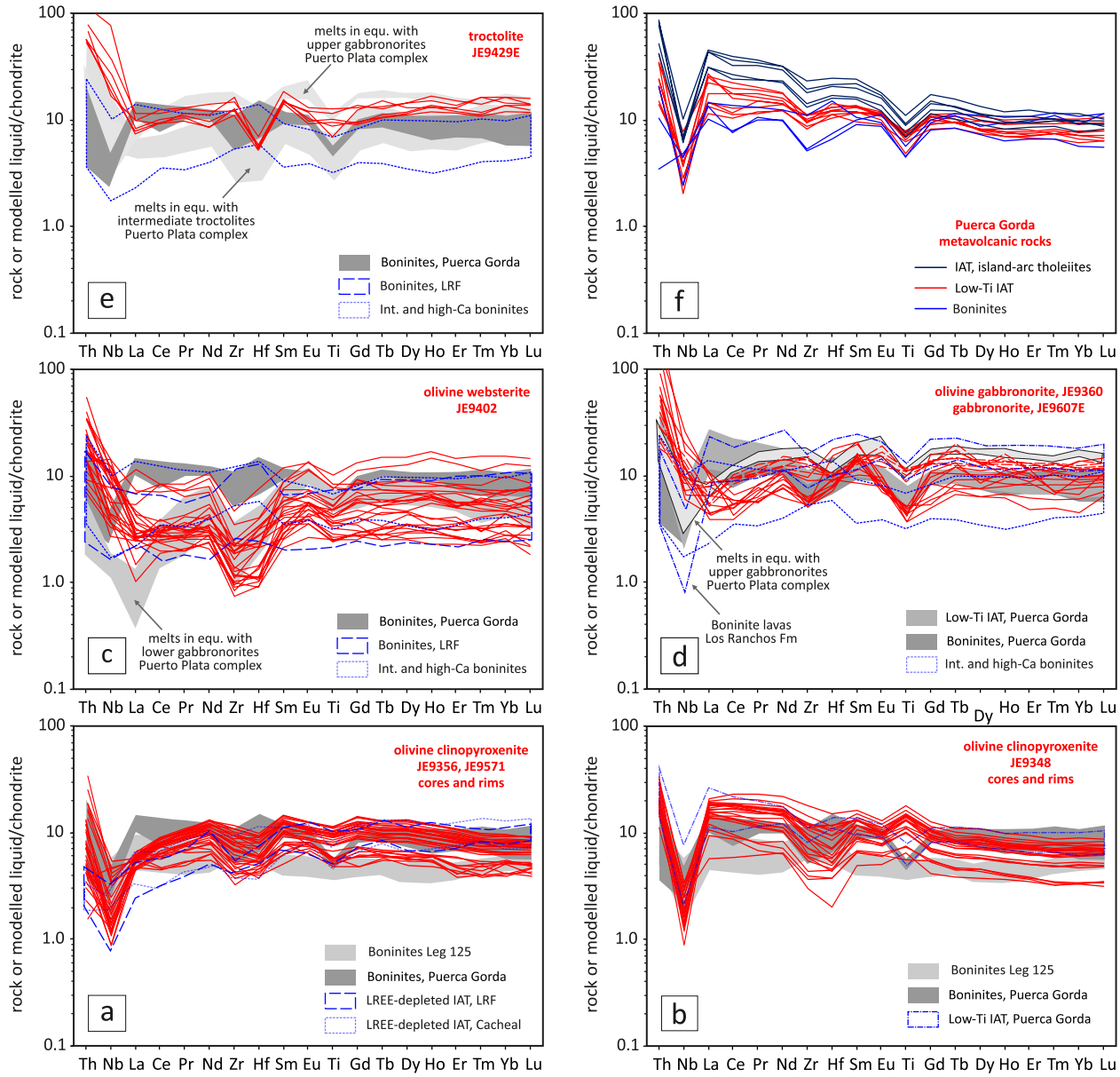

Figure 11. Chondrite-normalized trace element patterns of calculated liquids (red lines) in equilibrium with mafic and ultramafic rocks of the Rio Boba plutonic sequence. (a, b and c) Pyroxenites, (d) gabbronorites, (e) troctolites, (f) Puerca Gorda metavolcanic rocks. The fields for volcanic rocks of the Puerca Gorda, Los Ranchos Formation (LR Fm), and Cacheal Complex of the Caribbean island-arc are from Escuder-Viruete, Friedman, et al. (2011) and Escuder-Viruete et al. (2006, 2014). Field for intermediate- and high-Ca boninites is from Crawford et al. (1989), Pearce et al. (1992), Pearce and Peate (1995), and Taylor et al. (1994). See text for explanation.

equilibrium with intermediate troctolites of the Puerto Plata complex, suggesting that they are genetically linked. The nature of the troctolites indicate that the parental magma, if it was boninitic, was high-Ca type, which is the least depleted of the boninite subtypes of Crawford et al. (1989). This interpretation is supported by HFSE and REE in the troctolites, which are similar to those of the intermediate and high-Ca boninite lavas (Figure 11d).

In summary, model melts provide a genetic link between the plutonic rocks (pyroxenite, gabbronorite, and troctolite) and Puerca Gorda metavolcanic rocks (Figure 11f). Thus, the ultramafic and mafic cumulates crystallized in equilibrium with melts in the lower crust. The melts were extracted and erupted to produce the volcanic sequence in the upper crust. The composition of model melts in equilibrium with more primitive clinopyroxenites and gabbronorites closely resemble those of LREE-depleted IAT and intermediate to high-Ca boninites. The

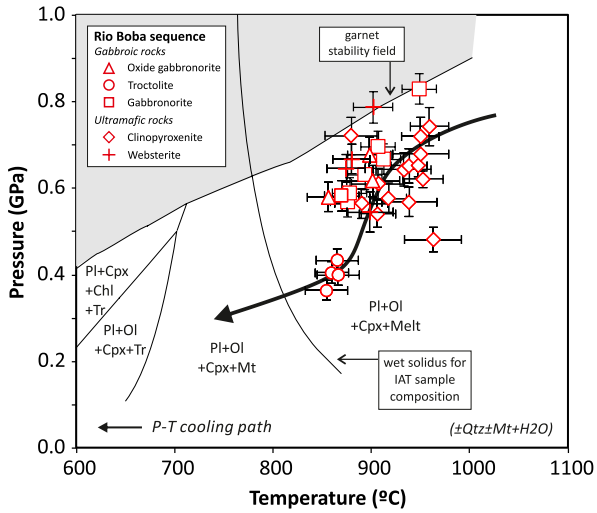

Figure 12. Equilibration P-T conditions for the pyroxenites and gabbroic rocks from two-pyroxene thermometry and the enstatite-in-cpx barometry (Putirka, 2008, 2018). Error bars are 1σ. Calculated temperatures are consistent with sub-solidus recrystallization. Equilibrium assemblage diagram in the NCKFMASH system is calculated for a model IAT bulk-rock geochemistry at H2O-saturated conditions (Escuder-Viruete & Pérez-Estaún, 2013). The black arrow indicates the P-T path followed during the cooling of the Rio Boba plutonic sequence.

crystallisation order of the Rio Boba mafic-ultramafic sequence with An-rich plagioclase after Mg-rich olivine, spinel, and pyroxene is consistent with the phenocrysts mineralogy observed in primitive and SiO_2-rich boninites (e.g., Taylor et al., 1994). The extremely low TiO_2, HFSE, and HREE in boninitic melts are commonly attributed to their derivation from a refractory mantle source (e.g., Pearce et al., 1992). The probable preserved remains of such refractory mantle are the basal harzburgite lenses found in tectonic contact with the underlying Cuaba unit (Figure 2; Escuder-Viruete & Castillo-Carrión, 2016). The LILE enrichment characteristic of Rio Boba plutonic sequence and Puerca Gorda volcanic rocks is typical of boninites and has been related to the addition of a component produced by dehydration and eventually partial melting of a subducted slab and/or overlying sediments (Bédard, 1999; Crawford et al., 1989; Falloon et al., 2008; Pearce & Reagan, 2019; Pearce et al., 1992; Tollstrup et al., 2010).

6.4. Origin of the Pyroxenite Bodies

Pyroxenites have been described from a number of arc crust and mantle environments (e.g., Berly et al., 2006). Arc crustal pyroxenites are interpreted as medium to high-pressure, ultramafic cumulates formed in mid to lower crustal magma chambers, some spanning the crust-mantle boundary at the base of an arc (e.g., DeBari & Greene, 2011). Mantle-derived pyroxenites differ from arc crustal pyroxenites in that they generally include a large variety of rock types ranging from orthopyroxenite through websterite to clinopyroxenite (Berly et al., 2006; Garrido & Bodinier, 1999).

In the Rio Boba plutonic sequence, the lithological contact between pyroxenite bodies and gabbronorites could not be observed due to the absence of outcrops. However, the magmatic layering in the pyroxenites suggests that the layering was originally sub-horizontal. Likewise, magmatic layering in the adjacent, overlying gabbronorite was originally horizontal to subhorizontal, both at the outcrop and regional scales. Therefore, the layering in the pyroxenite is parallel to the layering in the gabbronorite. These relationships suggest that the pyroxenites form as sub-horizontal sills, whose upward transition to the gabbronorites was controlled by gravity settling during magmatic crystal fractionation. The subhorizontal arrangement of the pyroxenite sills is therefore magmatic and represents the intrusion geometry of the sills during their emplacement in the lower arc crust. The observed centimeter-thick subvertical intrusions of pyroxenites in the gabbronorites represent magmatic conduits or feeder dikes (Figure 3f).

The clinopyroxenites and websterites of the Rio Boba sequence are characterized by a mineralogy similar to that of arc-crustal pyroxenites. Although their olivine compositions are primitive, they do not correspond to the higher Mg# and NiO-rich compositions observed in the olivine of the SSZ mantle peridotites of La Cuaba unit and the Puerto Plata ophiolite complex. (Figure 6). The Mg# values from orthopyroxene and clinopyroxene are lower than in mantle peridotites (Mg# >90), but similar to those of the more primitive gabbronorites. The absence of replacement textures precludes an origin through reaction between a peridotite and a circulating metasomatic agent (aqueous fluid and/or melt). These relationships suggest that the pyroxenite bodies were magma conduits along which primitive mantle-derived melts had risen through the crust-mantle transition into the lower crust and the basal part of large gabbroic sills. The gabbroic sills would form the lower crust of the arc, through multiple pulses of magma injection and fractionation.

6.5. Conditions of Formation of the Mafic-Ultramafic Sequence

The coexistence of magmatic clinopyroxene and orthopyroxene provides an estimation of the pressure-temperature conditions of equilibration of the pyroxenites and gabbronorites, using the two-pyroxene thermometer and the enstatite-in-cpx barometer of Putirka (2008; updated in 2018). Calculated equilibrium temperatures for the pyroxenites and gabbronorites range from 854°C to 962°C (Figure 12). Average temperatures calculated for clinopyroxenites (932°C ± 32°C), websterites (889°C ± 13°C), troctolites (861°C ± 5°C), gabbronorites

(921°C ± 20°C), and oxide gabbronorites (882°C ± 25°C), are within error, probably not distinguishable, and provide evidence for subsolidus recrystallization at 840°C–930°C. These subsolidus temperatures are consistent with the occurrence of lobate grain boundaries, which are indicative of dynamic recrystallization at relatively high-temperatures (Passchier & Trouw, 2005).

However, the presence of exsolution textures in the pyroxenes of the pyroxenites and gabbroic rocks evidence a previous higher-temperature crystallization/cooling history. To estimate the temperature of crystallization, the composition of the original pyroxene was calculated from the complementary lamellae exsolutions. The area corresponding to the exsolutions relative to the host pyroxene was determined by analyzing images of grains displaying exsolution lamellae. Then the relative areas were combined with EMPA spot analyses of the individual phases to recalculate the pyroxene composition prior to exsolution. For amounts between 4% and 10% of orthopyroxene exsolution lamellae in clinopyroxene, the calculated temperature of crystallisation is significantly higher, as high as 950°C–1078°C in the clinopyroxenites and websterites, and 928°C–1024°C in the troctolites and gabbronorites. These crystallization temperatures for the original clinopyroxene are consistent with the experimental results of the fractional crystallization of anhydrous tholeiitic liquids in the temperature range between 1,060°C and 1,330°C (at 0.7 GPa; Villiger et al., 2007).

The coronitic shells of orthopyroxene around olivine and symplectites of clinopyroxene + green spinel and/or amphibole + spinel between olivine and plagioclase, record the subsolidus cooling of the Rio Boba plutonic sequence from the granulite-to amphibolite-facies metamorphic conditions. Microstructural relationships, multiequilibrium thermobarometry and pseudosection analysis (in the NCKFMASH model system) suggest a P-T evolution of near isobaric cooling initially at ∼0.7 GPa, accompanied by an increase in H_2O activity (Figure 12; Escuder-Viruete, 2010). Microtextural relationships indicate that all these simplectites develop in both pyroxenites and gabbroic rocks after high-T ductile deformation (see below).

The barometric calculations establish equilibrium pressures between 0.36 and 0.83 GPa (Figure 12). These results are consistent with the absence of magmatic garnet in the Rio Boba plutonic sequence, and indicate that crystallization took place entirely at pressures below the stability limit of this mineral, which are of 0.6–0.8 GPa for temperatures of 800°C–1,000°C (at $P_{H2O} \sim P_{tot}$; Figure 12). Average pressures calculated for clinopyroxenites (0.61 ± 0.1 GPa), websterites (0.63 ± 0.1 GPa), gabbronorites (0.76 ± 0.13 GPa), and oxide gabbronorites (0.64 ± 0.05 GPa) are similar within error, but clearly higher than those obtained for the troctolites (0.4 ± 0.03 GPa). This suggest that the late intrusion of the troctolites took place at lower pressures (P ∼ 0.4 GPa), after the intrusion and ductile deformation at high-T of the pyroxenites and gabbronorites. This in turn has implications in the establishment of the magmatic evolution.

6.6. Magmatic Evolution of the Rio Boba Plutonic Sequence and Puerca Gorda Metavolcanic Rocks

The field, structural, petrological and geochemical data suggest a magmatic evolution in three stages for the Rio Boba plutonic sequence and Puerca Gorda metavolcanic rocks. Therefore, the genetic link between ultramafic and mafic sequences in the Caribbean arc crust is complex and indicates a multi-stage evolution. The first stage is the formation of an arc crustal substrate as the result of melting a refractory mantle source, represented by the cumulate sequence of pyroxenites and gabbronorites. Modeling suggests that melts in equilibrium with these rocks would have erupted as the variably LREE-depleted and low-Ti IAT and boninitic volcanic protoliths of the Puerca Gorda Schists, among which there is probably a compositional transition. Low LREE contents, small negative Nb, and positive Th anomalies indicate that the subduction component was, if present, small in this initial stage. Sub-horizontal ductile stretching, deformative fabrics and recrystallization microstructures indicates that this mafic-ultramafic substrate was heterogeneously deformed at mid-P granulite to upper amphibolite metamorphic facies conditions. Although the outcrop conditions do not allow determining its spatial distribution, this deformation seems to be located preferentially at the higher structural levels of the plutonic sequence (i.e., the Matel gabbronorites).

The second stage included the volumetrically subordinate troctolites, which preserve igneous cumulate textures, have a boninitic geochemical affinity and are not penetratively deformed. According to modeling, these would be associated with some of the Puerca Gorda boninitic protoliths. The mantle source is refractory and enriched by a LILE-rich hydrous fluid, and possibly by a LREE-rich melt, derived from a subducting slab and/or overlying

sediments (Bédard, 1999; Falloon et al., 2008; Pearce et al., 1992). Regionally, the troctolites have provided a U-Pb zircon age of 126.1 ± 1.3 Ma, therefore constraining the high-T deformation to pre-126 Ma times.

The third stage is recorded in the supra-crustal section of the arc by the Puerca Gorda Schist, no record of this latter stage has been found in the Rio Boba gabbroic rocks. The third stage encompassed the "normal" IAT volcanic protoliths with higher Th and higher LREE and a pronounced negative Nb anomaly. These volcanic rocks indicate that the source of tholeiitic magmas became enriched by a strong subduction component.

In summary, the magmatic evolution of the Rio Boba sequence is multi-stage, and involves the formation of magmas from melting of different mantle sources in a supra-subduction zone with a progressive involvement of a subduction component. The evolution constitutes the basis for a tectono-magmatic model for the Caribbean island arc proposed hereafter.

6.7. Tectono-Magmatic Model for the Caribbean Island Arc in Northern Hispaniola

Much of the plutonic and volcanic rocks of the Caribbean island arc in northern Hispaniola have a depleted geochemical signature, in particular the boninitic rocks (e.g., Escuder-Viruete et al., 2006). This depleted nature results from melting of a refractory mantle source, from which melts had previously been extracted (i.e., they are "second-stage melts"; Bédard, 1999; Crawford et al., 1989; Falloon et al., 2008, Pearce & Reagan, 2019; Pearce et al., 1992). The temperatures required for melting a refractory mantle to produce boninites (1,100°C–1,550°C) are higher than those expected in a typical sub-arc mantle wedge. Several processes, in specific tectonic settings, have been proposed to explain such elevated temperatures (see review in Pearce & Reagan, 2019). Among these geodynamic contexts, a possible scenario for the generation of boninites in the Caribbean island arc involves subduction initiation (Escuder-Viruete et al., 2014). The absence of a previous intra-oceanic arc indicates that boninitic magmas did not form by arc or fore-arc rifting or propagation of a spreading center into an arc.

Boninite magmatism is commonly linked to embryonic arc volcanism following intra-oceanic subduction initiation, as has been proposed for the Eocene boninites in the Izu-Bonin-Mariana fore-arc (Reagan et al., 2019; Stern, 2010; Taylor et al., 1994). In this area, subduction initiation was followed by the creation of oceanic crust by a seafloor spreading, where compositions evolved from tholeiitic basalt ("fore-arc basalt") to (low-Si) boninite (Ishizuka et al., 2006, 2011; Reagan et al., 2010, 2019). This was followed by construction of a protoarc of predominantly boninitic (high-Si boninite) composition, as the residual mantle from the spreading event undergoes second-stage melting induced by flux of fluids and melts from the newly formed subducting plate (e.g., Pearce & Reagan, 2019; Taylor et al., 1994). Stabilization of subduction and advection of more fertile mantle to the fusion zone gives rise, via transitional compositions, to the beginning of normal tholeiitic arc magmatism (Ishizuka et al., 2011; Leng et al., 2012; Stern & Gerya, 2018).

In this context, a tectono-magmatic model for the evolution of the Caribbean island arc is proposed in Figure 13, inspired by the geometry for subduction initiation driven by internal vertical forces of Maunder et al. (2020). Subduction was initiated in the Pacific realm during the Lower Cretaceous, probably along a weak zone in the oceanic crust (Figure 13a). This caused extension and stretching in the overriding plate, leading to eventual breakup. During this stage (Figure 13b), decompression melting was probably minor, due to a low geothermal gradient and the scarcity or absence of fluids (no subducting slab). These magmas generated new crust now preserved as the pyroxenites and gabbronorites of the Rio Boba sequence and the lower gabbronorites of the Puerto Plata ophiolite complex. Complementary volcanic rocks are the LREE-depleted IAT of Puerca Gorda, Cacheal and Los Ranchos Formation. These rocks lack a significant geochemical subductive component because the transfer of trace elements from the subducting slab to the mantle wedge must have been limited during the arc infancy (e.g., Dhuime et al., 2009). Extension in the upper Caribbean plate produced sub-horizontal ductile stretching and mid-P upper amphibolite to granulite-facies metamorphism in the lower arc crust, recorded in the heterogeneous deformation fabrics and recrystallization microstructures preserved in the gabbronorites. In the Puerto Plata ophiolite complex, the volcanic upper crust is structurally disrupted probably, by low-angle detachment faulting similar to that occurring in oceanic core complexes along mid-ocean ridges (e.g., Escartın et al., 2008).

Once subduction started (Figure 13c), the associated rollback led to an immediate influx of hot mantle from below (Stern, 2010). At this stage, boninitic magmas would have formed when the depleted mantle reached a level where it was fluxed with fluids and/or melts derived from the subducted slab. These magmas continue to form crust in the form of the gabbronorites and troctolites of the Rio Boba and Puerto Plata ophiolite complex.

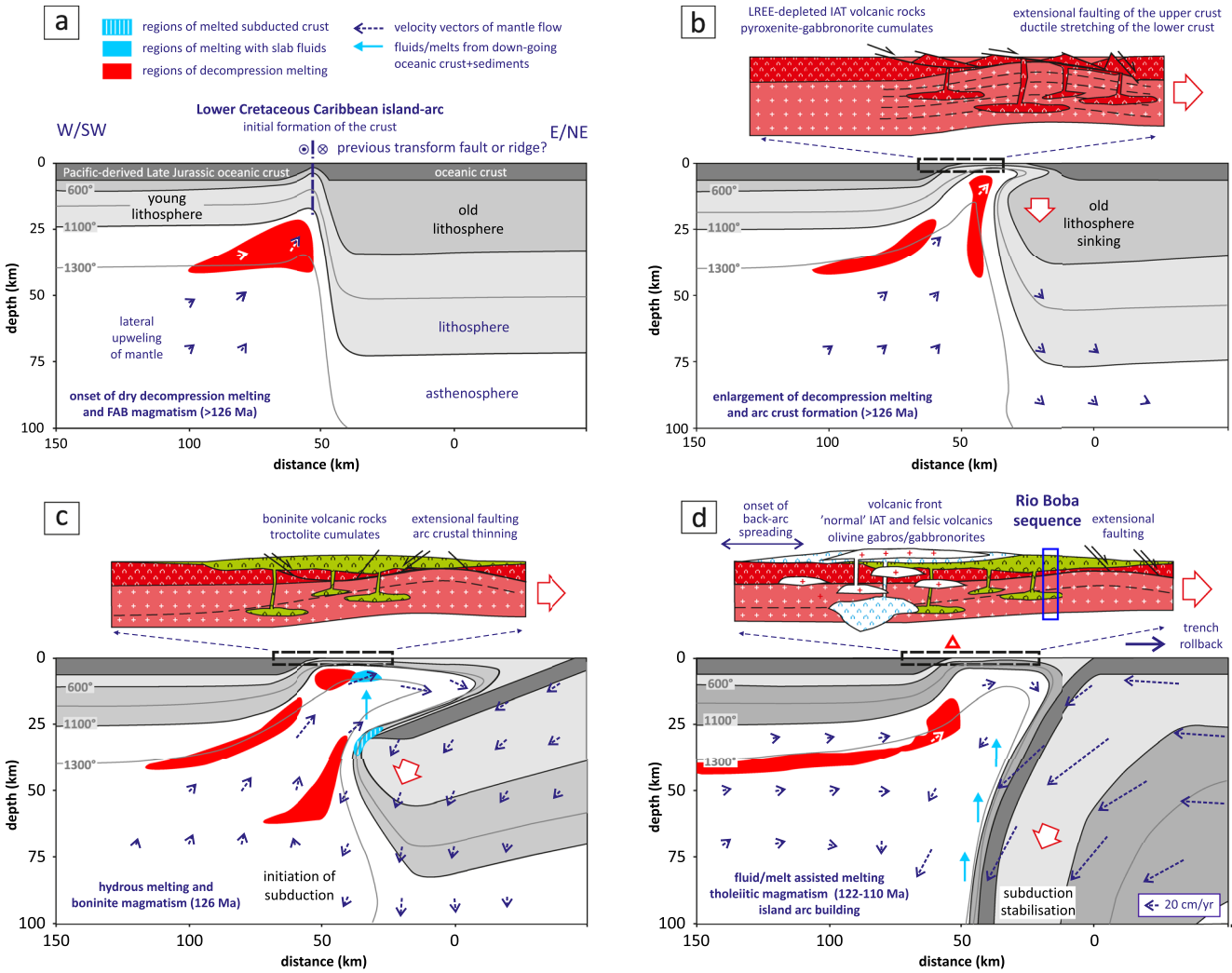

Figure 13. Tectono-magmatic model for the evolution of the Caribbean island arc magmatism. It is inspired in the modeling of the Izu-Bonin-Marianas subduction system (Maunder et al., 2020). Stages: (a) subduction initiation, (b) extension and decompression melting, (c) oceanic subduction an rollback, and (d) IAT magmatism. Subduction initiation took place in response to the sinking of the oldest and thickest lithosphere in the mantle, which originated an asthenospheric upwelling and a lithospheric "gap" beneath the old transform fault. The temperature profiles show the regions where decompression melting and melting in the presence of slab fluids occurred, and where subducting crust crossed its solidus. Above each temperature profile, the evolution of magmatism in the Caribbean island arc is shown schematically. See text for explanation.

Regionally related volcanic rocks are the boninite protoliths of the Puerca Gorda Schists and the boninite lavas of the Los Ranchos Formation and Cacheal complex. This change in magmatism is not abrupt, since there is a continuous compositional transition between LREE-depleted IAT and boninite. Subduction initiation must have occurred prior to 126 Ma, the age of the intermediate troctolites of boninitic affinity. This scenario is consistent with the undeformed nature of the troctolites and their late placement at pressures of approximately 0.4 GPa, suggesting a vertical uplift of 6–9 km of the host pyroxenites and gabbronorites, related to extensional tectonics, prior to the troctolite intrusion.

As extension proceeded, the fertile mantle may have decompressed enough to initiate melting. This effect would have been amplified if the rising fertile mantle entered the region of the mantle wedge that was fluxed by fluids expelled from the subducting slab (Figure 13d). As the convergence rate and subduction angle stabilized, reorganization of the asthenospheric circulation caused the fore-arc to cool and forced the magmatic axis to retreat (Ishizuka et al., 2006, 2011; Reagan et al., 2010, 2019; Stern, 2010). This process may have yielded "normal" tholeiitic SSZ magmas, which generated the upper olivine gabbros and gabbronorites in the PPC. Regionally related volcanic rocks are the IAT of the Puerca Gorda, Los Caños and Los Ranchos Formations, and El Cacheal

complex. This magmatic stage is apparently not recorded in the Rio Boba sequence, probably due to its position close to the trench and far from the volcanic front, located to the southwest (~200 km from the trench in the Izu-Bonin-Mariana arc). The presence of more evolved andesites and dacites-rhyolites in the upper stratigraphic levels of the Los Ranchos Formation suggests that the Caribbean island arc matured during this magmatic stage (Escuder-Viruete et al., 2006; Kesler et al., 2005; Lewis et al., 2002).

Experimental data show that large ultramafic cumulates can form by fractional crystallization of up to 50% of primary, mantle-derived melts, crystallizing as pyroxenites prior to plagioclase saturation at the base of the crust (e.g., Villiger et al., 2004). However, this sequence of ultramafic cumulates is missing at the exposed base of the Caribbean island arc. The relatively small ultramafic bodies intruded into the lower crustal gabbronorites of the Rio Boba sequence only represent ~5% of the outcrop area. The lack of the expected cumulate sequence indicates that the base of the Caribbean island arc was significatively disturbed during, or slightly after, the main stage of arc crustal building. This may reflect delamination of dense, unstable lower crust comprising ultramafic cumulates (Jull & Kelemen, 2001), or convective thermomechanical erosion of the sub-arc lithosphere (Kelemen et al., 2014). As shown schematically in Figure 13d, mantle corner flow enhanced by pervasive hydration of the mantle wedge may account for upper plate thinning (down to 30 km thick) in a relatively short time span of 15–25 Ma, from the beginning of arc building to cessation. Both processes, however, would account for the high temperature conditions required for dehydration/melting of the lower arc section. Hornblende tonalite melts produced during this melting event were intruded at shallow crustal levels into the volcanic rocks of Los Ranchos Formation at 116–115 Ma (Escuder-Viruete et al., 2006). $^{40}Ar/^{39}Ar$ plateau ages of hornblende in most tonalites are Albian (109–106 Ma) and interpreted as final cooling ages, prior to unroofing and erosion of the inactive Caribbean arc, which is unconformably covered in the upper Lower Albian by the reef limestones of the Hatillo Formation.

Finally, the basal part of the Rio Boba plutonic sequence experienced ductile deformation, mylonitization and amphibolite facies retrograde metamorphism in the 88–84 Ma interval, before tectonic juxtaposition to the Cuaba unit along the Jobito detachment zone in the 82–70 Ma interval. The surface exposure and erosion of the sequence in the Maastrichtian-lower Eocene is related to collision of the Caribbean plate with the North American continental margin, which took place at about 60 ± 5 Ma (see Escuder-Viruete, Pérez-Estaún, Booth-Rea, et al., 2011; Escuder-Viruete, Pérez-Estaún, Gabites, et al., 2011).

Data Availability Statement

The data for this paper are contained in the text, figures and Supporting Information and can also be found in the ESSOAr (Earth and Space Science Open Archive; Escuder-Viruete et al., 2022).

Acknowledgments
The authors wish to thank Gren Draper for their comments on the geology of the Dominican Republic. The authors would also like to thank support and infrastructure provided by the Servicio Geológico Nacional of the Dominican Republic, particularly to Santiago Muñoz. The collaboration in some fieldwork of Pol Uriane, Jacques Monthel, Ángela Suárez, and Alberto Díaz de Neira is much appreciated. Part of the analytical work had the invaluable help of Martin Robyr, Alexey Ulianov, Claudia Baumgartner, and Peter O. Baumgartner of the ISTE, Université de Lausanne. Richard Abbott provided a careful review of a first version of the manuscript. Constructive reviews by two anonymous reviewers, as well as the editorial work by Yamirka Rojas-Agramonte and Claudio Faccenna, significantly improved the manuscript. This research was funded through CGL2012-33669/BTE and PID2019-105625RB-C22 of the MCIN/AEI/10.13039/501100011033 projects and PRX18/00055 stay grant to the J. Escuder-Viruete of the Ministerio de Ciencia e Innovación of the Spanish Government.

References

Abbott, R. N., Jr., Broman, B. N., & Draper, G. (2007). UHP magma paragenesis revisited, olivine clinopyroxenite, and garnet-bearing ultramafic rocks from the Cuaba Gneiss, Rio San Juan complex, Dominican Republic. *International Geology Review*, *49*, 572–586. https://doi.org/10.2747/0020-6814.49.6.572

Abbott, R. N., Jr., & Draper, G. (2013). The case for UHP conditions in the Cuaba Terrane, Rio San Juan metamorphic complex, Dominican Republic. *Geológica Acta*, *11*, 149–165.

Alonso-Perez, R., Müntener, O., & Ulmer, P. (2009). Igneous garnet and amphibole fractionation in the roots of island arcs: Experimental constrains on H_2O undersaturated andesitic liquids. *Contributions to Mineralogy and Petrology*, *157*, 541–558. https://doi.org/10.1007/s00410-008-0351-8

Arculus, R., Ishizuka, O., Bogus, K., Gurnis, M., Hickey-Vargas, R., Aljahdali, M. H., et al. (2015). A record of spontaneous subduction initiation in the Izu–Bonin–Mariana arc. *Nature Geoscience*, *8*, 728–733. https://doi.org/10.1038/ngeo2515

Beccaluva, L., Macciotta, G., Picardo, G. B., & Zeda, O. (1989). Clinopyroxene compositions of ophiolite basalts as petrogenetic indicator. *Chemical Geology*, *77*, 165–182. https://doi.org/10.1016/0009-2541(89)90073-9

Bédard, J. H. (1999). Petrogenesis of Boninites from the Betts Cove Ophiolite, Newfoundland, Canada: Identification of subducted source components. *Journal of Petrology*, *40*, 1853–1889. https://doi.org/10.1093/petroj/40.12.1853

Bédard, J. H. (2005). Partitioning coefficients between olivine and silicate melts. *Lithos*, *83*, 394–416. https://doi.org/10.1016/j.lithos.2005.03.011

Berly, T. J., Hermann, T., Arculus, R. J., & Lapierre, H. (2006). Supra-subduction zone Pyroxenites from San Jorge and Santa Isabel (Solomon Islands). *Journal of Petrology*, *47*(8), 1531–1555. https://doi.org/10.1093/petrology/egl019

Bodinier, J. L., & Godard, M. (2007). Orogenic, Ophiolitic, and Abyssal Peridotites. In H. D. Holland & K. K. Turekian (Eds.), *Treatise on geochemistry* (pp. 1–73). Pergamon. https://doi.org/10.1016/B0-08-043751-6/02004-1

Bouilhol, P., Schmidt, M., & Burg, J. P. (2015). Magma transfer and evolution in channels within the arc crust: The pyroxenitic feeder pipes of Sapat (Kohistan, Pakistan). *Journal of Petrology*, *56*, 1309–1342. https://doi.org/10.1093/petrology/egv037

Burg, J. P. (2011). The Asia-Kohistan-India collision. Review and discussion. In D. Brown & P. Ryan (Eds.), *Arc-continent collision: The making of an orogeny. Frontiers in Earth Sciences* (pp. 279–309). Springer. https://doi.org/10.1007/978-3-540-88558-0_10

Calvert, A. J. (2011). The seismic structure of island arc crust. In D. Brown & P. Ryan (Eds.), *Arc-continent collision: The making of an orogeny. Frontiers in Earth Sciences* (pp. 87–120). Springer.

Crawford, A. J., Falloon, T. J., & Green, D. H. (1989). Classification, petrogenesis and tectonic setting of boninites. In A. J. Crawford (Ed.), *Boninites and related rocks* (pp. 1–49). Unwin Hyman London.

DeBari, S. M., & Greene, A. R. (2011). Vertical Stratification of composition, density, and Inferred magmatic Processes in exposed arc crustal Sections. In D. Brown & P. Ryan (Eds.), *Arc-continent collision: The making of an orogeny. Frontiers in Earth Sciences* (pp. 121–144). Springer. https://doi.org/10.1007/978-3-540-88558-0_5

Dhuime, B., Bosch, D., Bodinier, J. L., Garrido, C. J., Bruguier, O., Hussain, S. S., & Dawood, H. (2007). Multistage evolution of the Jijal ultramafic–mafic complex (Kohistan, N Pakistan): Implications for building the roots of island arcs. *Earth and Planetary Science Letters*, *261*, 179–200. https://doi.org/10.1016/j.epsl.2007.06.026

Dhuime, B., Bosch, D., Garrido, C. J., Bodinier, J. L., Bruguier, O., Hussain, S. S., & Dawood, H. (2009). Geochemical architecture of the lower- to middle-crustal Section of a Paleo-island Arc (Kohistan complex, Jijal-Kamila Area, Northern Pakistan): Implications for the evolution of an oceanic subduction zone. *Journal of Petrology*, *50*, 531–569. https://doi.org/10.1093/petrology/egp010

Draper, G., Mann, P., & Lewis, J. F. (1994). Hispaniola. In S. K. Donovan & T. A. Jackson (Eds.), *Caribbean geology: An introduction* (pp. 129–150). Jamaica, University of the West Indies Publishers Association.

Draper, G., & Nagle, F. (1991). Geology, structure, and tectonic development of the Río San Juan complex, northern Dominican Republic. In P. Mann, G. Draper, & J. F. Lewis (Eds.), *Geologic and tectonic development of the North America-Caribbean plate boundary in Hispaniola* (Vol. 62, pp. 77–95). Geological Society of America Special Paper. https://doi.org/10.1130/spe262-p77

Escartın, J., Smith, D. K., Cann, J., Schouten, H., Langmuir, C. H., & Escrig, S. (2008). Central role of detachment faults in accretion of slow-spread oceanic lithosphere. *Nature*, *455*, 790–794. https://doi.org/10.1038/nature07333

Escuder-Viruete, J. (2010). *Informe: Petrología de Rocas Ígneas y Metamórficas, Hojas de Río San Juan, Guayabito, Salcedo, Gaspar Hernández, Pimentel, Cabrera y Villa Riva* (p. 91). Mapa Geológico de la República Dominicana Escala 1:50.000. Servicio Geológico Nacional. Retrieved from https://www.sgn.gob.do

Escuder Viruete, J., Beranoaguirre, A., Valverde-Vaquero, P., & Mcdermott, F. (2020). Quaternary deformation and uplift of coral reef terraces produced by oblique subduction and underthrusting of the Bahama Platform below the northern Hispaniola forearc. *Tectonophysics*, *796*, 228631. https://doi.org/10.1016/j.tecto.2020.228631

Escuder-Viruete, J., & Castillo-Carrión, M. (2016). Subduction of fore-arc crust beneath an intra-oceanic arc: The high-P Cuaba mafic gneisess and amphibolites of the Rio San Juan complex, Dominican Republic. *Lithos*, *262*, 298–319. https://doi.org/10.1016/j.lithos.2016.07.024

Escuder-Viruete, J., Castillo-Carrión, M., Gabites, J., Súarez, A., & Pérez-Estaún, A. (2014). Magmatic relations of Caribbean upper mantle peridotites, lower crustal gabbroic rocks and upper crustal basaltic lavas: Geochemical constraints from the Puerto Plata ophiolite complex, Northern Hispaniola. *Lithos*, *196–197*, 261–280. https://doi.org/10.1016/j.lithos.2014.03.013

Escuder-Viruete, J., Castillo-Carrión, M., Pérez Valera, F., Valverde-Vaquero, P., Rubio Ordónez, Á., & Fernández, F. J. (2022). *Cumulate layered gabbronorites and pyroxenites of the Rio Boba plutonic sequence, northern Dominican Republic [Preprint]*. https://doi.org/10.1002/essoar.10507766.1

Escuder-Viruete, J., Díaz de Neira, A., Hernáiz Huerta, P. P., Monthel, J., García Senz, J., Joubert, M., et al. (2006). Magmatic relationships and ages of Caribbean island arc tholeiites, boninites and related felsic rocks, Dominican Republic. *Lithos*, *90*, 161–186. https://doi.org/10.1016/j.lithos.2006.02.001

Escuder-Viruete, J., Friedman, R., Castillo-Carrión, M., Gabites, J., & Pérez-Estaún, A. (2011). Origin and significance of the ophiolitic high-P mélanges in the northern Caribbean convergent margin: Insights from the geochemistry and large-scale structure of the Río San Juan metamorphic complex. *Lithos*, *127*, 483–504. https://doi.org/10.1016/j.lithos.2011.09.015

Escuder-Viruete, J., & Pérez, Y. (2020). Neotectonic structures and stress fields associated with oblique collision and forearc sliver formation in northern Hispaniola: Implications for the seismic hazard assessment. *Tectonophysics*, *784*, 228452. https://doi.org/10.1016/j.tecto.2020.228452

Escuder-Viruete, J., & Pérez-Estaún, A. (2013). Contrasting exhumation P–T paths followed by high-P rocks in the northern Caribbean subduction–accretionary complex: Insights from the structural geology, microtextures and equilibrium assemblage diagrams. *Lithos*, *160–161*, 117–144. https://doi.org/10.1016/j.lithos.2012.11.028

Escuder-Viruete, J., Pérez-Estaún, A., Booth-Rea, G., & Valverde-Vaquero, P. (2011). Tectonometamorphic evolution of the Samaná complex, northern Hispaniola: Implications for the burial and exhumation of high-pressure rocks in a collisional accretionary wedge. *Lithos*, *125*, 190–210. https://doi.org/10.1016/j.lithos.2011.02.006

Escuder-Viruete, J., Pérez-Estaún, A., Gabites, J., & Suárez-Rodríguez, Á. (2011). Structural development of a high-pressure collisional accretionary wedge: The Samaná complex, northern Hispaniola. *Journal of Structural Geology*, *33*, 928–950. https://doi.org/10.1016/j.jsg.2011.02.006

Escuder-Viruete, J., Valverde-Vaquero, P., Rojas-Agramonte, Y., Gabites, J., & Pérez-Estaún, A. (2013). From intra-oceanic subduction to arc accretion and arc-continent collision: Insights from the structural evolution of the Río San Juan metamorphic complex, northern Hispaniola. *Journal of Structural Geology*, *46*, 34–56. https://doi.org/10.1016/j.jsg.2012.10.008

Escuder-Viruete, J., Valverde-Vaquero, P., Rojas-Agramonte, Y., Jabites, J., Carrión-Castillo, M., & Pérez-Estaún, A. (2013). Timing of deformational events in the Río San Juan complex: Implications for the tectonic controls on the exhumation of high-P rocks in the northern Caribbean subduction-accretionary prism. *Lithos*, *177*, 416–435. https://doi.org/10.1016/j.lithos.2013.07.006

Falloon, T. J., & Crawford, A. J. (1991). The petrogenesis of high calcium boninite lavas from the northern Tonga ridge. *Earth and Planetary Science Letters*, *102*, 375–394.

Falloon, T. J., Danyushevsky, L. V., Crawford, A. J., Meffre, S., Woodhead, J. D., & Bloomer, S. H. (2008). Boninites and adakites from the northern termination of the Tonga Trench: Implications for adakite petrogenesis. *Journal of Petrology*, *49*, 697–715. https://doi.org/10.1093/petrology/egn009

Garrido, C. J., & Bodinier, J. L. (1999). Diversity of mafic rocks in the Ronda peridotite: Evidence for pervasive melt–rock reaction during heating of subcontinental lithosphere by upwelling asthenosphere. *Journal of Petrology*, *40*, 729–754. https://doi.org/10.1093/petroj/40.5.729

Garrido, C. J., Bodinier, J. L., Burg, J. P., Zeilinger, G., Hussain, S. S., Dawood, H., et al. (2006). Petrogenesis of mafic garnet granulite in the lower crust of the Kohistan paleo-arc complex (Northern Pakistan): Implications for intra-crustal differentiation of island arcs and generation of continental crust. *Journal of Petrology*, *47*, 1873–1914. https://doi.org/10.1093/petrology/egl030

Garrido, C. J., Bodinier, J. L., Hussain, S. S., Dawood, H., & Burg, J. P. (2007). Origin of the island arc Moho transition zone via melt-rock reaction and its implications for intracrustal differentiation of island arcs: Evidence from the Jijal complex (Kohistan complex, Northern Pakistan). *Geology*, *35*(8), 683–686. https://doi.org/10.1130/g23675a.1

Gazel, E., Abbott, R. N., & Draper, G., Jr. (2011). Garnet-bearing ultramafic rocks from the Dominican Republic: Fossil mantle plume fragments in an ultra-high pressure oceanic complex? *Lithos*, *125*, 393–404. https://doi.org/10.1016/j.lithos.2011.02.021

Greene, A. R., DeBari, S. M., Kelemen, P. B., & Clift, P. D. (2006). A detailed geochemical study of island arc crust: The Talkeetna arc section, south-central Alaska. *Journal of Petrology*, *47*(6), 1051–1093. https://doi.org/10.1093/petrology/egl002

Hastie, A. R., Mitchell, S. F., Treloar, P. J., Kerr, A. C., Neill, I., & Barfod, D. N. (2013). Geochemical components in a Cretaceous island arc: The Th/La–(Ce/Ce*)Nd diagram and implications for subduction initiation in the inter-American region. *Lithos*, *162–163*, 57–69. https://doi.org/10.1016/j.lithos.2012.12.001

Hattori, K. H., Guillot, S., Saumur, B.-M., Tubrett, M. N., Vidal, O., & Morfin, S. (2010). Corundum-bearing garnet peridotite from northern Dominican Republic: A metamorphic product of an arc cumulate in the Caribbean subduction zone. *Lithos*, *114*, 437–450. https://doi.org/10.1016/j.lithos.2009.10.010

Hattori, K. H., Guillot, S., Tubrett, M. N., Saumur, B. M., Vidal, O., & Morfin, S. (2010). Reply to comment on "Corundum-bearing garnet peridotites from northern Dominican Republic: A metamorphic product of an arc cumulate in the Caribbean subduction zone" by Richard N. Abbott and Grenville Draper. *Lithos*, *117*, 322–326. https://doi.org/10.1016/j.lithos.2010.03.007

Hochstaedter, A., Gill, J., Peters, R., Broughton, P., Holden, P., & Taylor, B. (2001). Across-arc geochemical trends in the Izu-Bonin arc: Contributions from the subducting slab. *Geochemistry, Geophysics, Geosystems*, *2*. https://doi.org/10.1029/2009GC002847

Ishikawa, T., Nagaishi, K., & Umino, S. (2002). Boninitic volcanism in the Oman ophiolite: Implications for thermal condition during transition from spreading ridge to arc. *Geology*, *30*, 899–902. https://doi.org/10.1130/0091-7613(2002)030<0899:bvitoo>2.0.co;2

Ishizuka, O., Kimura, J. I., Li, Y. B., Stern, R. J., Reagan, M. K., Taylor, R. N., et al. (2006). Early stages in the evolution of Izu-Bonin arc volcanism: New age, chemical and isotope constrains. *Earth and Planetary Science Letters*, *250*, 385–401. https://doi.org/10.1016/j.epsl.2006.08.007

Ishizuka, O., Tani, K., Reagan, M. K., Kanayama, K., Umino, S., Harigane, Y., et al. (2011). The timescales of subduction initiation and subsequent evolution of an oceanic island arc. *Earth and Planetary Science Letters*, *306*, 229–240. https://doi.org/10.1016/j.epsl.2011.04.006

Jagoutz, O., Bouilhol, P., Schaltegger, U., & Müntener, O. (2018). The isotopic evolution of the Kohistan Ladakh arc from subduction initiation to continent arc collision. In P. J. Treloar & M. P. Searle (Eds.), *Himalayan tectonics: A modern synthesis* (Vol. 483, pp. 165–182). Geological Society, London, Special Publications. https://doi.org/10.1144/sp483.7

Jagoutz, O., Muntener, O., Burg, J. P., Ulmer, P., Pettke, T., Burg, J. P., et al. (2007). Petrology and mineral chemistry of lower crustal Intrusions: The Chilas complex, Kohistan (NW Pakistan). *Journal of Petrology*, *48*(10), 1895–1953. https://doi.org/10.1093/petrology/egm044

Jagoutz, O., Müntener, O., Schmidt, M. W., & Burg, J. P. (2011). The roles of flux- and decompression melting and their respective fractionation lines for continental crust formation: Evidence from the Kohistan arc. *Earth and Planetary Science Letters*, *303*, 25–36. https://doi.org/10.1016/j.epsl.2010.12.017

Jagoutz, O., & Schmidt, M. W. (2012). The formation and bulk composition of modern juvenile continental crust: The Kohistan arc. *Chemical Geology*, *298–299*, 79–96. https://doi.org/10.1016/j.chemgeo.2011.10.022

Jolly, W. T., Lidiak, E. G., & Dickin, A. P. (2006). Cretaceous to mid-Eocene pelagic sediment budget in Puerto Rico and the Virgen Islands (northeast Antilles Island-arc). *Geológica Acta*, *4*, 35–62.

Jull, M., & Kelemen, P. B. (2001). On the conditions for lower crustal convective instability. *Journal of Geophysical Research*, *106*(B4), 6423–6446. https://doi.org/10.1029/2000jb900357

Kelemen, P. B., Hanghøj, K., & Greene, A. R. (2014). One view of the geochemistry of subduction-related magmatic arcs, with an emphasis on primitive andesite and lower crust. In H. D. Holland & K. K. Turekian (Eds.), *The crust, Treatise on Geochemistry* (pp. 669–701). Pergamon.

Kesler, S. E., Campbell, I. H., & Allen, C. M. (2005). Age of the Los Ranchos Formation, Dominican Republic: Timing and tectonic setting of primitive island arc volcanism in the Caribbean region. *The Geological Society of America Bulletin*, *117*, 987–995. https://doi.org/10.1130/b25594.1

Krebs, M., Schertl, H.-P., Maresch, W. V., & Draper, G. (2011). Mass flow in serpentinite-hosted subduction channels: P–T–t path patterns of metamorphic blocks in the Rio San Juan mélange (Dominican Republic). *Journal of Asian Earth Sciences*. https://doi.org/10.1016/j.jseaes.2011.01.011

Leat, P. T., & Larter, R. D. (2003). Intra-oceanic subduction systems: Introduction. In R. D. Larter & P. T. Leat (Eds.), *Intra-oceanic subduction systems: Tectonic and magmatic processes* (Vol. 219, pp. 1–17). Geological Society of London, Special Publications. https://doi.org/10.1144/gsl.sp.2003.219.01.01

Leng, W., Gurnis, M., & Asimow, P. (2012). From basalts to boninites: The geodynamics of volcanic expression during induced subduction initiation. *Lithosphere*, *4*, 511–523. https://doi.org/10.1130/l215.1

Lewis, J. F., Escuder Viruete, J., Hernáiz Huerta, P. P., Gutiérrez, G., Draper, G., & Pérez Estaún, A. (2002). Subdivisión geoquímica del Arco Isla Circum-Caribeño, Cordillera Central Dominicana: Implicaciones para la formación, acreción y crecimiento cortical en un ambiente intraoceánico. *Acta Geologica Hispanica*, *37*, 81–122.

Mann, P., Draper, G., & Lewis, J. F. (1991). An overview of the geologic and tectonic development of Española. In P. Mann, G. Draper, & J. F. Lewis (Eds.), *Geologic and tectonic development of the North America-Caribbean plate boundary in Española* (Vol. 262, pp. 1–28). Geological Society of America Special Paper.

Marchesi, C., Garrido, C. J., Godard, M., Proenza, J. A., Gervilla, F., & Blanco-Moreno, J. (2006). Petrogenesis of highly depleted peridotites and gabbroic rocks from the Mayarí-Baracoa Ophiolitic Belt (eastern Cuba). *Contributions to Mineralogy and Petrology*, *151*, 717–736. https://doi.org/10.1007/s00410-006-0089-0

Maunder, B., Prytulak, J., Goes, S., & Reagan, M. (2020). Rapid subduction initiation and magmatism in the Western Pacific driven by internal vertical forces. *Nature Communications*, *11*, 1874. https://doi.org/10.1038/s41467-020-15737-4

McInnes, B. I. A., Gregoire, M., Binns, R. A., Herzig, P. M., & Hannington, M. D. (2001). Hydrous metasomatism of oceanic sub-arc mantle, Lihir, Papua New Guinea: Petrology and geochemistry of fluid-metasomatised mantle wedge xenoliths. *Earth and Planetary Science Letters*, *188*, 169–183. https://doi.org/10.1016/s0012-821x(01)00306-5

Müntener, O., Kelemen, P. B., & Grove, T. L. (2001). The role of H_2O during crystallization of primitive arc magmas under uppermost mantle conditions and genesis of igneous pyroxenites: An experimental study. *Contributions to Mineralogy and Petrology*, *141*(6), 643–658. https://doi.org/10.1007/s004100100266

Müntener, O., & Ulmer, P. (2018). Arc crust formation and differentiation constrained by experimental petrology. *American Journal of Science*, *318*, 64–89. https://doi.org/10.2475/01.2018.04

Passchier, C. W., & Trouw, R. A. J. (2005). *Microtectonics* (p. 382). Springer.

Pearce, J. A. (2003). Supra-subduction zone ophiolites: The search for modern analogues. *Geological Society of America Special Paper*, *373*, 269–293. https://doi.org/10.1130/0-8137-2373-6.269

Pearce, J. A., & Peate, D. W. (1995). Tectonic implications of the composition of volcanic arc magmas. *Earth and Planetary Science Annual Rewiew*, *23*, 251–285. https://doi.org/10.1146/annurev.ea.23.050195.001343

Pearce, J. A., & Reagan, M. K. (2019). Identification, classification, and interpretation of boninites from Anthropocene to Eoarchean using Si-Mg-Ti systematics. *Geosphere*, *15*(4), 1008–1037. https://doi.org/10.1130/ges01661.1

Pearce, J. A., van der Laan, S. R., Arculus, R. J., Murton, B. J., Ishii, T., Peate, D. W., & Parkinson, I. J. (1992). Boninite and harzburgite from Leg 125 (Bonin-Mariana Fore-arc): A case study of magma genesis during the initial stages of subduction. In P. Fryer, J. A. Pearce, & L. B. Stocking (Eds.), *Proceedings ocean drilling program, scientific results* (Vol. 125, pp. 623–659). https://doi.org/10.2973/odp.proc.sr.125.172.1992

Pérez-Estaún, A., Hernaiz Huerta, P. P., Lopera, E., Joubert, M., Escuder Viruete, J., Díaz de Neira, A., et al. (2007). Geología de la República Dominicana: De la construcción de arco-isla a la colisión arco-continente. *Boletin Geologico y Minero*, *118*, 157–174.

Proenza, J. A., Díaz-Martínez, R., Iriondo, A., Marchesi, C., Melgarejo, J. C., Gervilla, F., et al. (2006). Primitive Cretaceous island-arc volcanic rocks in eastern Cuba: The teneme formation. *Geológica Acta*, *4*, 103–121.

Putirka, K. (2008). Thermometers and Barometers for volcanic Systems. In K. Putirka & F. Tepley (Eds.), *Minerals, inclusions and volcanic processes, reviews in mineralogy and geochemistry* (Vol. 69, pp. 61–120). Mineralogical Society America. https://doi.org/10.1515/9781501508486-004

Putirka, K. (2018). *Clinopyroxene-based Thermobarometers (Clinopyroxene_P-T_9-26-16)*. Retrieved from http://www.fresnostate.edu/csm/ees/documents/Clinopyroxene_P-T_9-26-16.xlsx

Reagan, M. K., Heaton, D. E., Schmitz, M. D., Pearce, J. A., Shervais, J. W., & Koppers, A. A. P. (2019). Forearc ages reveal extensive short-lived and rapid seafloor spreading following subduction initiation. *Earth and Planetary Science Letters*, *506*, 520–529. https://doi.org/10.1016/j.epsl.2018.11.020

Reagan, M. K., Ishizuka, O., Stern, R. J., Kelley, K. A., Ohara, Y., Blichert-Toft, J., et al. (2010). Fore-arc basalts and subduction initiation in the Izu-Bonin-Mariana system. *Geochemistry, Geophysics, Geosystems*, *11*, Q03X12. https://doi.org/10.1029/2009GC002871

Rioux, M., Hacker, B., & Mattinson, J. (2007). Magmatic development of an intra-oceanic arc: High-precision U-Pb zircon and whole-rock isotopic analyses from the accreted Talkeetna arc, south-central Alaska. *The Geological Society of America Bulletin*, *119*(9–10), 1168–1184. https://doi.org/10.1130/b25964.1

Rojas-Agramonte, Y., Garcia-Casco, A., Kemp, A., Kröner, A., Proenza, J. A., Lázaro, C., & Liu, D. (2016). Recycling and transport of continental material through the mantle wedge above subduction zones: A Caribbean example. *Earth and Planetary Science Letters*, *436*, 93–107. https://doi.org/10.1016/j.epsl.2015.11.040

Rojas-Agramonte, Y., Kröner, A., Garcia-Casco, A., Somin, M., Iturralde-Vinent, M. A., Mattinson, J. M., et al. (2011). Timing and evolution of Cretaceous island arc magmatism in Central Cuba: Implications for the history of arc system in the Northwestern Caribbean. *The Journal of Geology*, *119*, 619–640. https://doi.org/10.1086/662033

Saccani, E., & Photiades, A. (2004). Mid-ocean ridge and supra-subduction affinities in the Pindos massif ophiolites (Greece): Implications for magma genesis in a proto-forearc setting. *Lithos*, *73*, 229–253. https://doi.org/10.1016/j.lithos.2003.12.002

Santos, J. F., Schärer, U., Gil Ibarguchi, J. I., & Girardeau, J. (2002). Genesis of pyroxenite-rich peridotite at Cabo Ortegal (NW Spain): Geochemical and Pb–Sr–Nd isotope data. *Journal of Petrology*, *43*, 17–43. https://doi.org/10.1093/petrology/43.1.17

Stern, R. J. (2010). The anatomy and ontogeny of modern intra-oceanic arc systems. In T. M. Kusky, M.-G. Zhai, & W. Xiao (Eds.), *The evolving continents: Understanding processes of continental growth* (Vol. 338, pp. 7–34). Geological Society Special Publications.

Stern, R. J., & Gerya, T. (2018). Subduction initiation in nature and models: A review. *Tectonophysics*, *746*, 173–198. https://doi.org/10.1016/j.tecto.2017.10.014

Stern, R. J., Reagan, M., Ishizuka, O., Ohara, Y., & Whattam, S. A. (2012). To understand subduction initiation, study forearc crust: To understand forearc crust, study ophiolites. *Lithosphere*, *4*, 469–483. https://doi.org/10.1130/l183.1

Sun, S. S., & McDonough, W. F. (1989). Chemical and isotopic systematics of oceanic basalts: Implications for mantle compositions and processes. In A. D. Saunders & M. J. Norry (Eds.), *Magmatism in the ocean basins* (Vol. 42, pp. 313–345). Geological Society Special Publication. https://doi.org/10.1144/gsl.sp.1989.042.01.19

Takahashi, N., Kodaira, S., & Tatsumi, Y. (2008). Structure and growth of the Izu-Bonin-Mariana arc crust: 1. Seismic constraint on crust and mantle structure of the Mariana arc–back-arc system. *Journal of Geophysical Research*. https://doi.org/10.1029/2007JB005120

Taylor, R. N., Nesbitt, R. W., Vidal, P., Harmon, R. S., Auvray, B., & Croudace, I. W. (1994). Mineralogy, chemistry, and genesis of the boninite series volcanics, Chichijima, Bonin Islands, Japan. *Journal of Petrology*, *35*, 577–617. https://doi.org/10.1093/petrology/35.3.577

Tollstrup, D., Gill, J., Kent, A., Prinkey, D., Williams, R., Tamura, Y., & Ishizuka, O. (2010). Across-arc geochemical trends in the Izu-Bonin arc: Contributions from the subducting slab, revisited. *Geochemistry, Geophysics, Geosystems*, *11*, Q01X10. https://doi.org/10.1029/2009GC002847

Torró, L., Proenza, J. A., Marchesi, C., García-Casco, A., & Lewis, J. F. (2017). Petrogenesis of meta-volcanic rocks from the Maimón Formation (Dominican Republic): Geochemical record of the nascent Greater Antilles paleo-arc. *Lithos*, *278–281*, 255–273. https://doi.org/10.1016/j.lithos.2017.01.031

Torró, L., Proenza, J. A., Rojas-Agramonte, Y., Garcia-Casco, A., Yang, J.-H., & Yang, Y.-H. (2018). Recycling in the subduction factory: Archaean to Permian zircons in the oceanic Cretaceous Caribbean island-arc (Hispaniola). *Gondwana Research*, *54*, 23–37. https://doi.org/10.1016/j.gr.2017.09.010

Tribuzio, R., Tiepolo, M., & Fiameni, S. (2008). A mafic–ultramafic cumulate sequence derived from boninite-type melts (Niagara Icefalls, northern Victoria Land, Antarctica). *Contributions to Mineralogy and Petrology*, *155*, 619–633. https://doi.org/10.1007/s00410-007-0261-1

Villiger, S., Ulmer, P., & Müntener, O. (2007). Equilibrium and fractional crystallization experiments at 0.7 GPa; the effect pf pressure on phase relations and liquid compositions of tholeiitic magmas. *Journal of Petrology*, *48*, 159–184.

Villiger, S., Ulmer, P., Müntener, O., & Thompson, A. B. (2004). The liquid line of descent of anhydrous mantle-derived, tholeiitic liquids by fractional crystallization and equilibrium crystallization – An experimental study at 1 GPa. *Journal of Petrology*, *45*, 2369–2388. https://doi.org/10.1093/petrology/egh042